

1

2 **Large DNA virus promoted the endosymbiotic evolution to make a photosynthetic**

3 **eukaryote**

4

5 **Authors and Affiliations**

6 Mitsuhiro Matsuo<sup>1</sup>, Atsushi Katahata<sup>1</sup>, Makoto Tachikawa<sup>1</sup>, Yohei Minakuchi<sup>2</sup>, Hideki

7 Noguchi<sup>3,4</sup>, Atsushi Toyoda<sup>2,4</sup>, Asao Fujiyama<sup>4</sup>, Yutaka Suzuki<sup>5</sup>, Takayuki Hata<sup>1</sup>,

8 Soichirou Satoh<sup>1</sup>, Takuro Nakayama<sup>6,7</sup>, Ryoma Kamikawa<sup>8</sup>, Mami Nomura<sup>8,9</sup>, Yuji

9 Inagaki<sup>6</sup>, Ken-ichiro Ishida<sup>9</sup>, Junichi Obokata<sup>1</sup>

10

11 <sup>1</sup>Graduate School of Life and Environmental Science, Kyoto Prefectural University,

12 Kyoto, 606-8522, Japan.

13 <sup>2</sup>Department of Genetics and Evolutionary Biology, National Institute of Genetics,

14 Mishima, Shizuoka, 411-8540, Japan.

15 <sup>3</sup>Center for Genome Informatics, Joint Support-Center for Data Science Research,

16 Research Organization of Information and Systems, Mishima, Shizuoka 411-8540,

17 Japan.

18 <sup>4</sup>Advanced Genomics Center, National Institute of Genetics, Mishima, Shizuoka

19 411-8540, Japan.

20 <sup>5</sup>Graduate school of Frontier Science, University of Tokyo, Kashiwa, Chiba, 272-8562,

21 Japan.

22 <sup>6</sup>Center for Computational Sciences, University of Tsukuba, Tsukuba, Ibaraki,

23 305-8577, Japan.

24 <sup>7</sup>Graduate School of Life Sciences, Tohoku University, Sendai 980-8578,

25 Japan

26 <sup>8</sup>Graduate Schools Human and Environmental Studies, Kyoto University, Kyoto,

27 606-8501, Japan.

28 <sup>9</sup>Graduate School of Life and Environmental Sciences, University of Tsukuba,

29 Tsukuba, Ibaraki, 305-8572, Japan.

30

31

32

33

34 **Abstract**

35 Chloroplasts in photosynthetic eukaryotes originated from a cyanobacterial  
36 endosymbiosis far more than 1 billion years ago<sup>1-3</sup>. Due to this ancientness, it remains  
37 unclear how this evolutionary process proceeded. To unveil this mystery, we analysed  
38 the whole genome sequence of a photosynthetic rhizarian amoeba<sup>4</sup>, *Paulinella*  
39 *micropora*<sup>5,6</sup>, which has a chloroplast-like organelle that originated from another  
40 cyanobacterial endosymbiosis<sup>7-10</sup> about 0.1 billion years ago<sup>11</sup>. Here we show that the  
41 predacious amoeba that engulfed cyanobacteria evolved into a photosynthetic organism  
42 very quickly in the evolutionary time scale, probably aided by the drastic genome  
43 reorganization activated by large DNA virus. In the endosymbiotic evolution of  
44 eukaryotic cells, gene transfer from the endosymbiont genome to the host nucleus is  
45 essential for the evolving host cell to control the endosymbiont-derived organelle<sup>12</sup>. In *P.*  
46 *micropora*, we found that the gene transfer from the free-living and endosymbiotic  
47 bacteria to the amoeba nucleus was rapidly activated but both simultaneously ceased  
48 within the initiation period of the endosymbiotic evolution, suggesting that the genome  
49 reorganization drastically proceeded and completed. During this period, large DNA

50 virus appeared to have infected the amoeba, followed by the rapid amplification and  
51 diversification of virus-related genes. These findings led us to re-examine the  
52 conventional endosymbiotic evolutionary scenario that exclusively deals with the host  
53 and the symbiont, and to extend it by incorporating a third critical player, large DNA  
54 virus, which activates the drastic gene transfer and genome reorganization between  
55 them. This *Paulinella* version of the evolutionary hypothesis deserves further testing of  
56 its generality in evolutionary systems and could shed light on the unknown roles of  
57 large DNA viruses<sup>13</sup> in the evolution of terrestrial life.

58

## 59 **Main manuscript**

60 Our laboratory culture of *P. micropora* MYN1<sup>5,6</sup> (Fig. 1a) is not axenic and  
61 contains bacteria. From this culture, we prepared the chromatins of *P. micropora* by  
62 micromesh-aided cell isolation and chromatin immunoprecipitation using a canonical  
63 histone antibody. Shotgun sequencing of this chromatin DNA gave us a high-quality  
64 draft genome assembly of 967 Mb (Fig. 1, Extended Data Fig. 1, Supplementary Table  
65 1). K-mer analysis estimated the genome size of *P. micropora* MYN1 to be 1.35 Gb

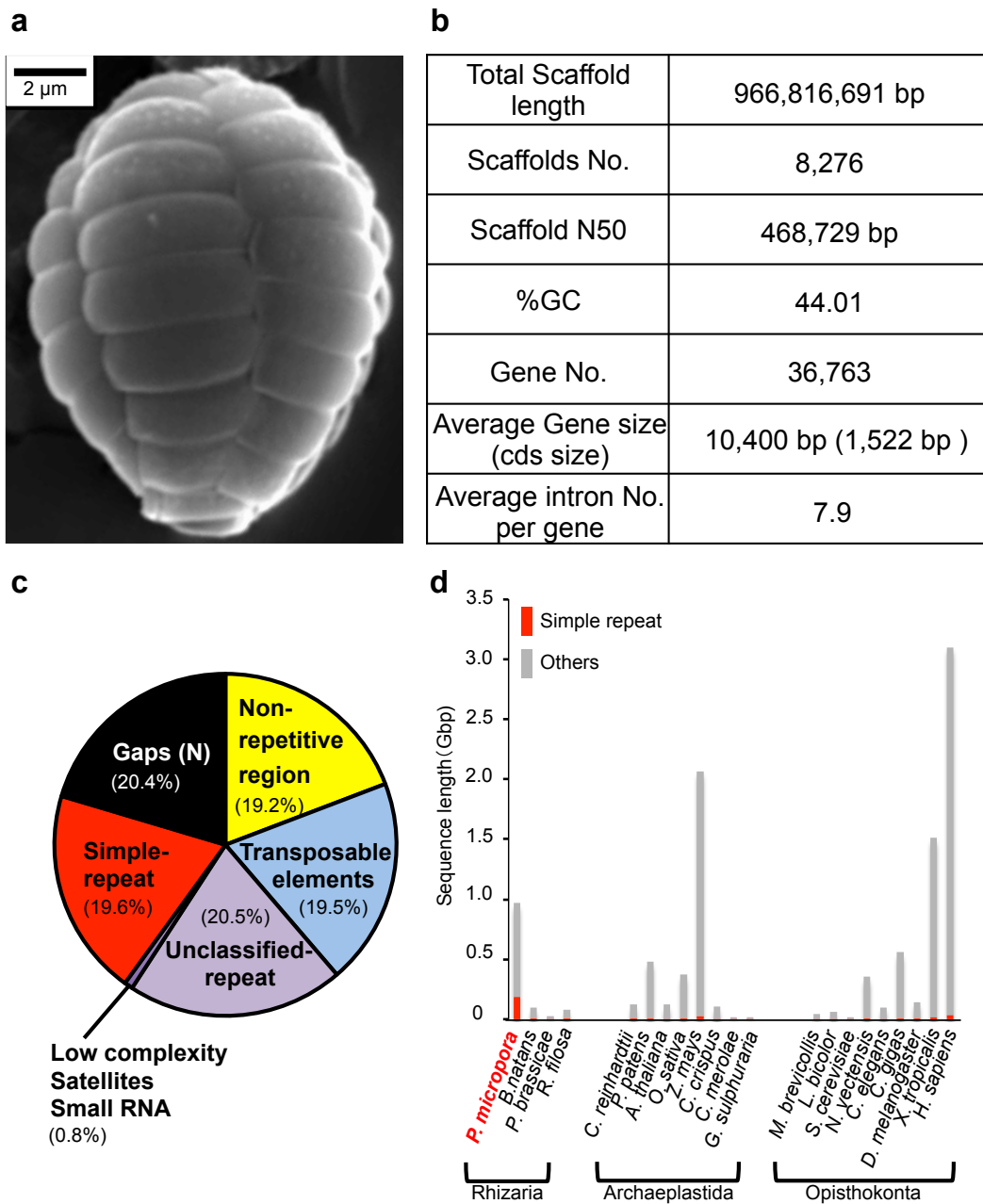


**Fig. 1. An overview of the *P. micropora* MYN1 draft genome. a,** A SEM image of *P. micropora* MYN1. **b,** The statistics of the draft genome. **c,** The genome composition of *P. micropora* MYN1 analysed by RepeatMasker<sup>27</sup>. **d,** Simple repeats are extraordinarily rich in *P. micropora* MYN1 compared with other organisms.

66 (Extended Data Fig. 1); hence, our draft assembly covered 72% of the whole genome.  
67 The genome is largely composed of repeated sequences, with 19.2% unique sequences  
68 (Fig. 1c). Simple repeat sequences are extraordinarily rich, amounting to 19.6% (Fig. 1c,  
69 1d). As much as simple repeats and transposons, 20.5% of the genome is occupied by  
70 unclassified repeat sequences that contain notable amounts of DNA virus-like fragments  
71 (Fig. 1c, Supplementary Table 2, 3).

72 A total of 36,763 protein gene models were predicted; on average, they were  
73 10.4 kb long and contained eight introns, implying large and complex structures (Fig.  
74 1b, Supplementary Table 4). Their gene ontology (GO) term analysis showed that  
75 DNA-related metabolism which associated with DNA virus is significantly  
76 over-represented compared with that of other rhizarian organisms (Extended Data Fig.  
77 1e, Supplementary Table 5).

78 From the above gene set of *P. micropora*, we attempted to characterize the  
79 genes that have been pivotal for the endosymbiotic evolution. We extracted the genes  
80 derived from cyanobacteria as well as those derived from the rest of the bacteria; we  
81 refer to the former as endosymbiotic gene transfer (EGT) candidates and the latter as

82 horizontal gene transfer (HGT) candidates in this study. We obtained 177 EGT and 248  
83 HGT candidates (Fig. 2, Supplementary Table 6). Half of the EGT candidates are genes  
84 for high light inducible proteins (HLIPs)<sup>12</sup>, which are involved in the protection against  
85 excess light energy. Phylogenetic analysis of these HLIPs showed that they are  
86 polyphyletic, suggesting that HLIPs should have been acquired by multiple independent  
87 gene transfers from cyanobacteria (Extended Data Fig. 2). Thus, the gain of a light  
88 protection system should have been crucial for the predacious amoeba to evolve into a  
89 photosynthetic organism.

90 HGT candidates contain genes of diverse functions, including ribosome  
91 biogenesis, DNA synthesis and amino acid metabolism. These genes appear to be  
92 involved in (1) endosymbiont biogenesis and (2) changes of the cellular nutrient state  
93 from heterotrophy to photo-autotrophy. To further examine the genes essential to the  
94 evolution of a photosynthetic organism, we compared orthologs among *P. micropora*,  
95 primary photosynthetic eukaryotes and predaceous eukaryotes (Extended Data Fig. 3a,  
96 3b); 12 orthologous groups are conserved in the former two but not in the latter,  
97 including the genes for light acclimation, organelle gene expression and changes of the

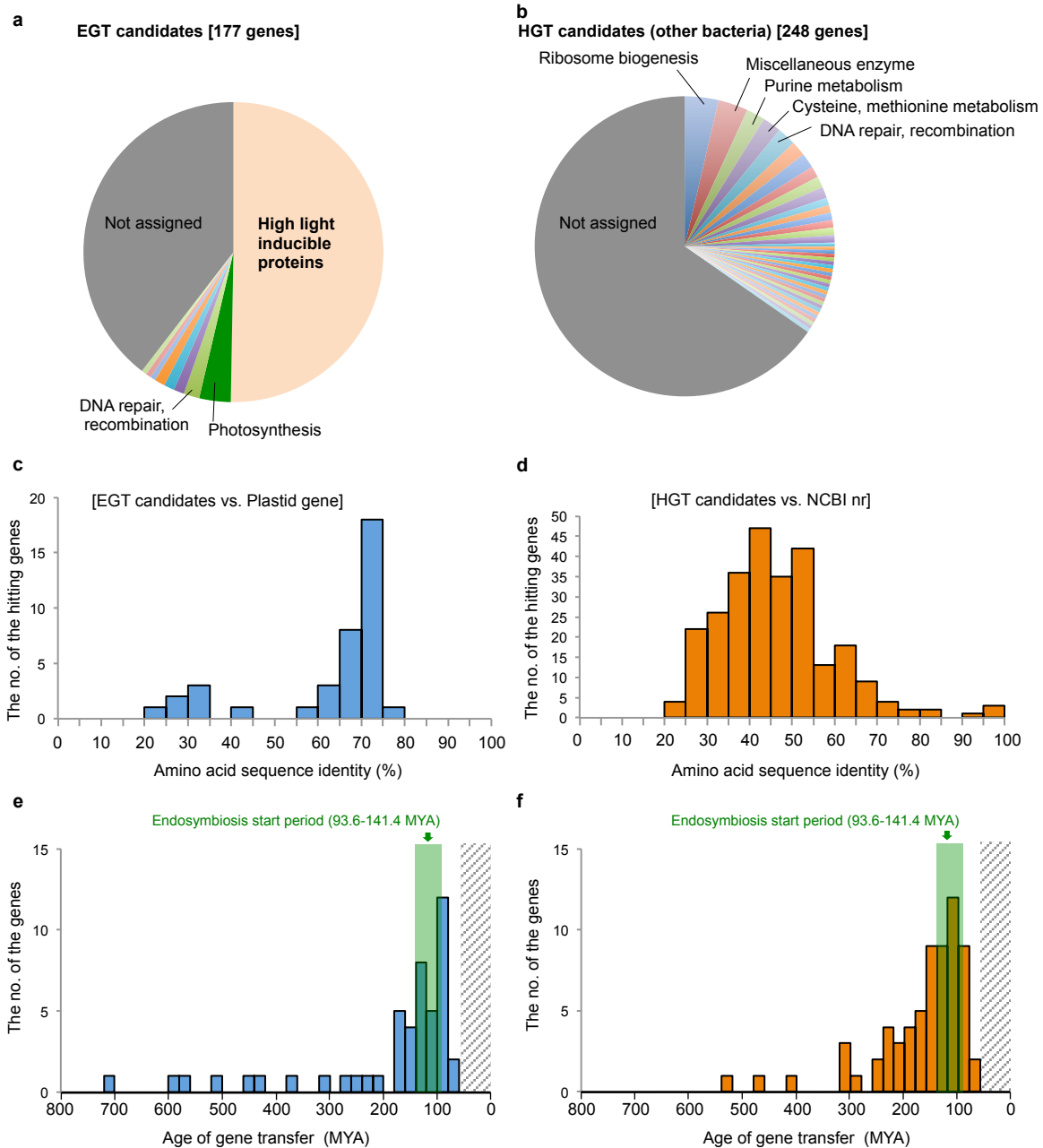


**Fig. 2. *P. micropora* nuclear genes acquired by EGT/HGT. a, b,** A functional classification of the *P. micropora* nuclear genes derived from cyanobacteria (EGT candidates) (a), and those from other bacteria (HGT candidates) (b). **c, d,** The amino acid sequence identity of EGT candidates against *P. micropora* MYN1 plastid genes (c) and that of HGT candidates against bacterial genes of the NCBI nr database (d). **e, f,** An estimation of the gene transfer age for EGT candidates (e) and HGT candidates (f). The endosymbiosis initiation period is green-highlighted. The ages of gene transfer in (e) and (f) were calculated based on the divergent time points (45.7–64.7 MYA) of two *Paulinella* species; thus, a gene transfer age younger than 60 MYA (striped phase) could not be estimated.



98 cellular nutrient state. Some of them were obtained horizontally from eukaryotes  
99 (Extended Data Figs. 3b–d). Therefore, *P. micropora* utilized the genes of diverse  
100 origins for endosymbiotic evolution.

101           The biggest challenge of this study is to elucidate the temporal sequence of  
102 the events that occurred at the birth of photosynthetic eukaryotes. To solve this puzzle,  
103 we first estimated how and when EGT occurred, based upon the sequence similarity  
104 between the EGT candidates and organelle-encoded genes. The results were surprising.  
105 We could not find any case with more than 80% amino acid sequence identity  
106 conserved between them (Fig. 2c), suggesting that plastidial EGT did not occur in a  
107 recent time period (Fig. 2e). We further searched for nuclear-localized plastid DNAs  
108 and nuclear-localized mitochondria DNAs<sup>15,16</sup> in the genome and found the latter but  
109 not the former. Therefore, it is likely that plastidial EGT rapidly activated and then  
110 ceased early in the endosymbiotic evolution in *P. micropora*, while this cool down was  
111 not found for mitochondrial EGT (Extended Data Fig. 4).

112           We confirmed this hypothesis from the different angle. Phylogenetic tree  
113 analysis of the EGT candidates showed that most of them already lost their counterparts

114 in the plastid genome, except for four genes; hence, we reckon that these four genes  
115 were transferred from the plastid to the nucleus relatively recently. The divergences of  
116 the four genes between their nuclear and plastid counterparts were estimated to have  
117 occurred 319.8 to 98.6 million years ago (MYA) (Extended Data Fig. 5). Considering  
118 that the photosynthetic *Paulinella* species have diverged from the heterotrophic species  
119 141.4 to 93.6 MYA<sup>11</sup>, even the latest EGT at 98.6 MYA had occurred within the  
120 initiation period of the endosymbiotic evolution. Taken together, the results of this  
121 study strongly suggest that EGT rapidly activated and ceased within the initial period of  
122 the endosymbiotic evolution (Fig. 2e), and a similar time course was also found for  
123 HGT (Fig. 2d, 2f).

124           What does this rapid and simultaneous cool-down of EGT and HGT (Figs.  
125 2c–2f) mean? The most simple and likely explanation is that the predaceous *Paulinella*  
126 shrank and lost phagocytic activity at this time to become a photosynthetic organism,  
127 accompanied by the shut-down of phagocytosis-aided EGT/HGT. In reality, HGT from  
128 prey cyanobacteria occurred in the predaceous *Paulinella* species<sup>17</sup>. If our assumption is  
129 correct, the predaceous *Paulinella* should have changed its cellular, genomic and

130 metabolic systems very quickly in terms of the evolutionary time scale. How was this  
131 drastic change possible? To examine this, we re-focused this study on DNA virus-like  
132 fragments frequently found in the *P. micropora* genome.

133           Fig. 3a shows a genomic scaffold containing putative virus fragments that are  
134 characterized by having from a dozen to a hundred copies, high GC content, ORFs  
135 similar to eukaryotic virus genes, and many intron-less genes of heterogeneous origins  
136 with unknown functions (Extended Data Fig. 6, Supplementary Table 3). In addition,  
137 they are often intermingled with simple repeats and mobile genetic elements, i.e.,  
138 Maverick/Polinton-type giant transposons<sup>18,19</sup> and retrotransposons. Most notably, the  
139 maximum fragment size reaches 300 kb (Extended Data Fig. 6). These structural  
140 features of the DNA virus-like fragments resemble those of nucleocytoplasmic large  
141 DNA viruses (NCLDV)<sup>20</sup> whose genome size ranges from 100 kbp to 2.5 Mbp and who  
142 have many genes of heterogeneous origins with unknown functions. However, a  
143 phylogenetic analysis based on DNA polymerases shows that those genes, encoded by  
144 the putative viral fragments, form a monophyletic clade distant from the genes of  
145 eukaryotes, prokaryotes and known NCLDVs (Fig. 3b). Therefore, we assume that they

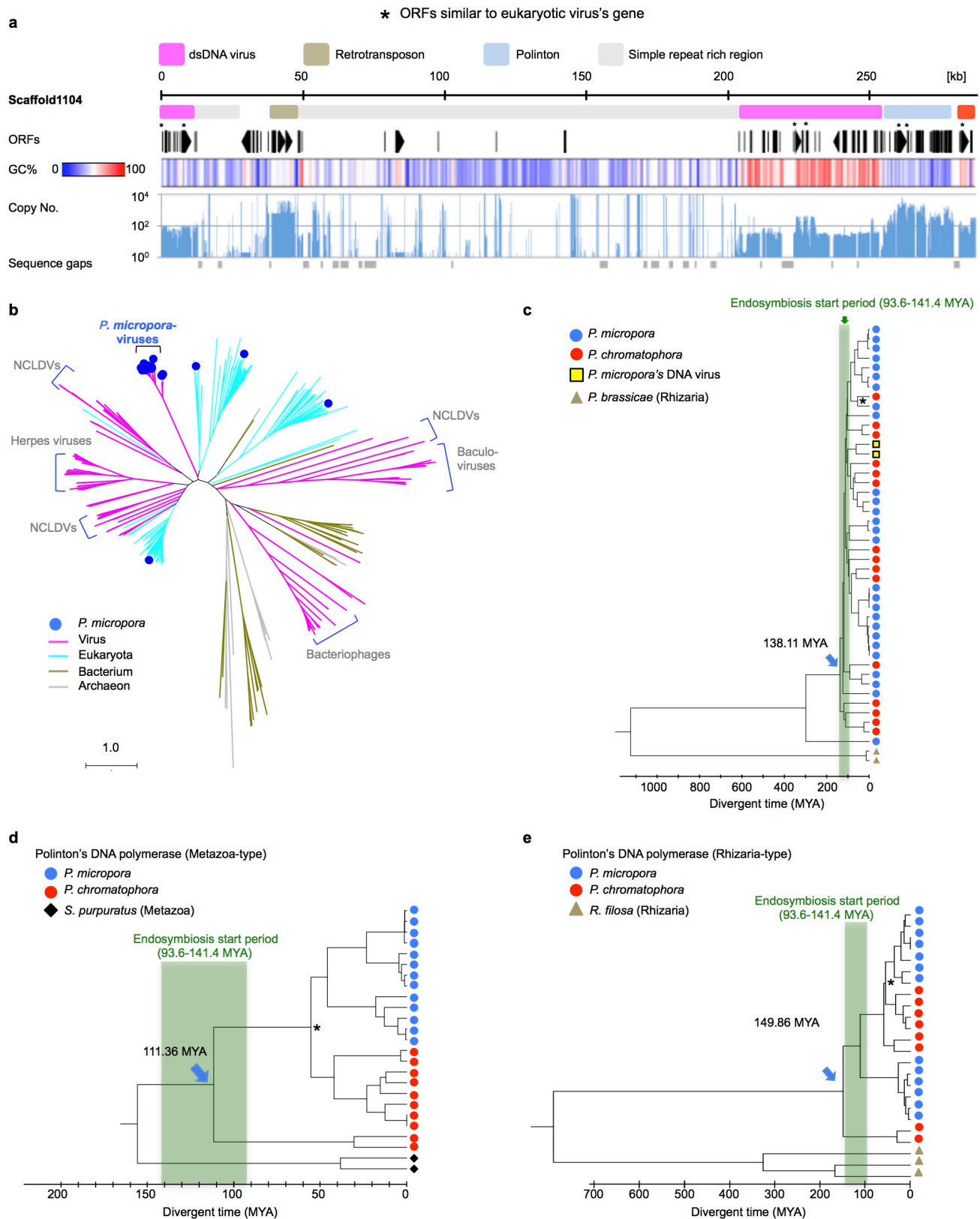


**Fig. 3. Putative DNA virus and mobile elements in *P. micropora* MYN1.** **a**, A schematic view of DNA virus-like fragments and mobile elements in the *P. micropora* draft genome (Scaffold 1104). The genomic regions were coloured according to the sequence characteristics; putative dsDNA virus (pink), Polinton (light blue), retrotransposon (brass yellow) and simple repeat-rich region (grey). The copy number of the interspersed repeat elements was analysed by BLASTN against the simple-repeat-masked *P. micropora* draft genome. **b**, ML phylogenetic tree of DNA polymerases of viruses, eukaryotes and prokaryotes. **c**, Divergent time analysis of the virus-type GPCR in *Paulinella*'s lineage. **d**, **e**, Divergent time analysis of DNA polymerase genes of metazoa-type (**d**) and rhizarian-type (**e**) Polintons. Asterisks: the branch point of *P. micropora* and *P. chromatophora* set at 45.7–64.7 MYA. Green bands: initiation periods of endosymbiosis with cyanobacteria (93.6–141.4 MYA). *P. micropora*; *Paulinella micropora* MYN1, *P. chromatophora*; *Paulinella chromatophora* CCAC0185, *P. brassicae*; *Plasmodiophora brassicae*, *R. filosa*; *Reticulomyxa filosa*, *S. purpuratus*; *Strongylocentrotus purpuratus*.

146 are from a novel large DNA virus but share several properties with known NCLDVs.

147 Our next question was when the putative virus infected the *Paulinella* lineage.

148 Although ancient infection hallmarks were already smeared, we found a suggestive case

149 in a *Paulinella*-specific gene family (Fig. 3c, Extended Data Fig. 7). The G-protein

150 coupled receptor (GPCR) genes rapidly expanded and diversified within a short

151 evolutionary period around the endosymbiosis initiation point. Noteworthy, two genes

152 of this family were found only in the putative viral fragment regions (yellow squares in

153 Fig. 3c and Extended Data Fig. 7). This suggests that these two genes diverged from the

154 rest of the family around the endosymbiosis initiation point and have been inherited

155 from the virus genome. This indicates that the putative virus has infected the *Paulinella*

156 lineage around the endosymbiosis initiation point or earlier.

157 To further prove this, we investigated the Maverick/Polinton-type transposons

158 derived from a virophage<sup>21</sup>, which parasitizes giant viruses (extremely large NCLDVs)

159 with its propagation depending on the host virus<sup>21,22</sup>. Virophages are also integrated into

160 the nuclear genome and could function as an anti-DNA virus system to protect

161 eukaryotic cells from the DNA virus<sup>23,24</sup>. Therefore, we hypothesized that the

162 emergence of Mavericks/Polintons and their amplifications have occurred concomitant  
163 with the DNA virus infection. In the *P. micropora* genome, two distinct  
164 Mavericks/Polintons, metazoan- and rhizaria-type, were detected in abundance  
165 (Extended Data Fig. 8, Supplementary Table 7). The divergent time analysis showed  
166 that both started amplification in the endosymbiosis initiation period (Fig. 3d, 3e).  
167 These results of the Maverick/Polinton-type transposons support the hypothesis that the  
168 large DNA virus infected the *Paulinella* lineage around the endosymbiosis initiation  
169 period.

170           Recent studies of NCLDV and giant DNA virus have drastically changed our  
171 conventional view of viruses<sup>13</sup>, especially their huge potential to incorporate diverse  
172 genetic materials of heterogenous origins<sup>25,26</sup> and to mediate their shuffling.  
173 Considering these properties of large DNA virus and the results of this study, we could  
174 reconstruct the initial evolutionary process of the photosynthetic *Paulinella* species as  
175 shown in Fig. 4. In this hypothetical model, large DNA virus contributed to the  
176 endosymbiotic evolution as a critical player, in addition to the original players of the  
177 host and symbiont. We should note that, in general, the detection of ancient infection

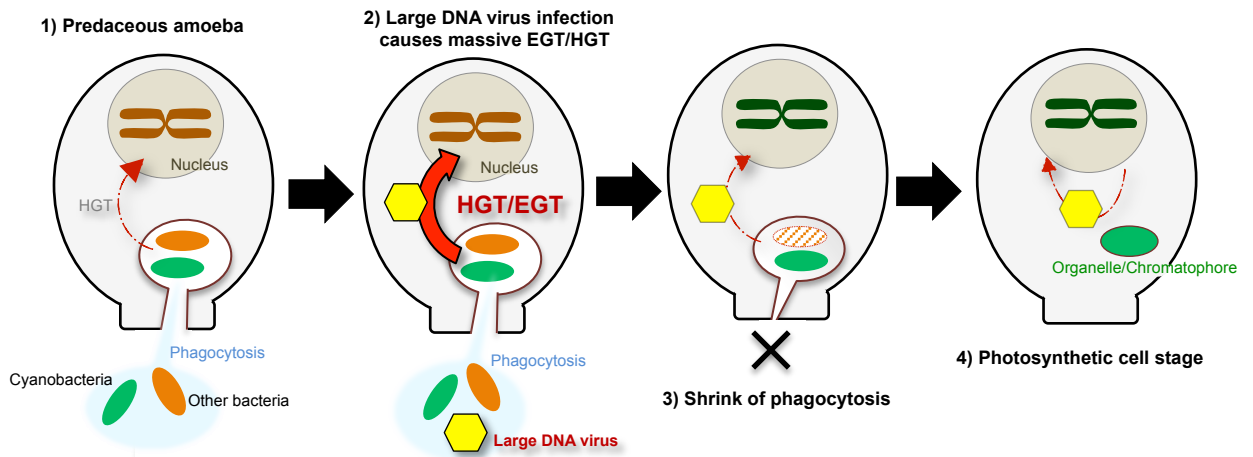


**Fig. 4. Initial process of the endosymbiotic evolution of photosynthetic *Paulinella* species modeled from the *P. micropora* genomic data.** 1) Predacious ancestors digested prey bacteria via phagocytosis with continuing low levels of HGT. 2) The infection of large DNA virus triggered the massive HGT/EGT to promote the rapid endosymbiotic evolution. 3) Acquiring photosynthetic competency shrunk the phagocytic activity to shut down the source of HGT/EGT. 4) The photo-autotrophic *Paulinella* sp. contains one photosynthetic organelle per cell, hence, release of the organelle DNA hardly occurred without losing photosynthetic activity. In this final stage, virus-mediated gene transfer continued at trace level.

178 hallmarks of large DNA virus seems difficult because (1) it could be easily lost due to  
179 its harmful and undesirable effects on host proliferation, (2) of poor information of the  
180 virus sequences and (3) of repeated sequences that are apt to be omitted in the assembly  
181 process of the genomic sequencing projects. This *Paulinella* version of the  
182 endosymbiotic evolution hypothesis deserves further examination to test its generality  
183 in many evolutionary systems.

184

## 185 **Methods**

### 186 **Data availability**

187 The sequences of the *P. micropora* draft genome, plastid (chromatophore) genome,  
188 mitochondria genome and the raw reads data set were deposited to the DDBJ  
189 (Accession No. are shown in Supplemental Table 8) and DDBJ reads archives (DRA  
190 Accession No. DRA003059, DRA003106, DRA008524).

191

192 ***P. micropora* culture and cell isolation.** The *P. micropora* MYN1 strain (NIES  
193 Collection, Tsukuba, JAPAN, NIES-4060) was cultured according to Nomura et al.



194 (2014)<sup>5</sup> and harvested by low-speed centrifugation ( $500 \times g$ , 2 min) at 4 °C. The  
195 harvested cells were resuspended in the culture medium and filtrated through a 20  $\mu\text{m}$   
196 mesh nylon filter (HD-20, Nippon Rikagaku Kikai Co., Ltd., Tokyo, Japan) to remove  
197 dead cell aggregates with high bacterial contamination. Recovered healthy cells were  
198 repeatedly washed with culture medium and subjected to RNA extraction. For  
199 extraction of chromatin DNA, the cells were subsequently washed three times with 10  
200 mM Tris-HCL (pH 8.0), six times with 10 mM Tris-HCL (pH 8.0) plus 10 mM EDTA,  
201 and recovered by a 5  $\mu\text{m}$  mesh nylon filter (PP-5n, Kyoshin Rikoh Inc., Tokyo, Japan)  
202 to give clean cells largely free of bacterial contamination.

203

204 **Chromatin and genomic DNA extraction.** Genomic DNA used for paired-end (300 b,  
205 500 b) and mate-pair (3 kb, 5 kb) libraries for HiSeq sequencing were purified by  
206 chromatin immunoprecipitation (ChIP) as follows. Ten milligrams of *P. micropora* cells  
207 were homogenized in 500  $\mu\text{l}$  homogenizing buffer (20 mM Tris-HCl (pH 7.6), 10 mM  
208 NaCl, 10 mM KCl, 2.5 mM EDTA, 250 mM sucrose, 0.1 mM spermine, 0.5 mM  
209 spermidine and 1 mM DTT) using a 30 $\mu\text{m}$  clearance glass homogenizer (RD440911,

210 Teraoka Co., Ltd., Osaka, Japan). After centrifugation ( $1000 \times g$ , 10 min,  $4^\circ\text{C}$ ), the  
211 pellets were resuspended in 300  $\mu\text{l}$  ChIP buffer (50 mM Tris-HCl (pH 8.0), 500 mM  
212 NaCl, 10 mM EDTA, 0.1% SDS, 0.5% Na-deoxycholate, 1% Triton X-100, 1 mM DTT  
213 and 10% glycerol) with 20  $\mu\text{l}$  Dynabeads protein G (Thermo Fisher Scientific, MA,  
214 U.S.A.) charged with 1  $\mu\text{g}$  anti-histone H3 antibody (Ab1791) ( Abcam plc, Cambridge,  
215 UK) and incubated at  $4^\circ\text{C}$  for 20 min. Dynabeads were then washed twice with ChIP  
216 buffer, twice with glycerol-free ChIP buffer and finally suspended in DNA extraction  
217 buffer (10 mM Tris-HCl (pH 8.0), 1 mM EDTA and 1% SDS). After RNase A (10  
218  $\mu\text{g}/\text{ml}$ ) and proteinase K (200  $\mu\text{g}/\text{ml}$ ) treatment, DNAs were purified by using Plant  
219 DNeasy Mini Kit (Qiagen, Hilden, Germany). For the construction of the long mate-pair  
220 libraries (12 kb, 15 kb, 18 kb and 20 kb), the total *P. micropora* genome was extracted  
221 without ChIP purification.

222

223 **Genome sequencing and assembly.** Sequencing libraries were prepared using a  
224 TruSeq DNA PCR-Free Library Preparation Kit and a Nextera Mate Pair  
225 Library Prep Kit (Illumina, San Diego, CA). Two paired-end libraries with

226 300 and 500bp inserts and six mate pair libraries (3kb, 5kb, 12kb, 15kb,  
227 18kb, and 20kb) were constructed and sequenced on the Illumina HiSeq  
228 2500 sequencers with 151 cycles per run. The nuclear draft genome was  
229 assembled by SOAPdenovo v2.04-r240<sup>28</sup> with a k-mer size of 121 after removing the  
230 sequence reads of the plastid (chromatophore) and mitochondria genomes, and those of  
231 two contaminating bacteria genomes. After the genome assembly, we checked for the  
232 contamination of the organelle genome and the bacteria genomes again, and we  
233 removed the contaminants from the draft genome. K-mer frequency analysis was  
234 performed by Jellyfish<sup>29</sup>. Genome scaffolds longer than 1 kb were analysed in this  
235 study.

236

237 **RNA-seq and Iso-Seq analysis.** RNAs were extracted from *P. micropora* cells at 0, 4,  
238 8, 12, 16 and 20 hr of 14L/10D photoperiod by Trizol® reagent (Thermo Fisher  
239 Scientific), and further purified using Plant RNeasy Mini Kit (Qiagen) with RNase-free  
240 DNase I treatment (Qiagen). Samples of the above time points were equally mixed and  
241 subjected to RNA-seq analysis using Agilent Strand Specific RNA Library Preparation

242 Kit (Agilent Technologies, CA, U.S.A) and Illumina HiSeq 2500 (Illumina). The paired  
243 end reads of RNA-seq were *de novo* assembled by Trinity<sup>30</sup> with the default setting or  
244 by CLC Genomics Workbench 7.0.3 (Qiagen) using a K-mer value of 54. The RNA-seq  
245 reads were mapped on the genome with Tophat<sup>31</sup> and assembled with Cufflinks<sup>32</sup> or  
246 Trinity<sup>30</sup>. For isoform-sequencing (Iso-Seq) of full-length transcripts, cDNAs were  
247 prepared from polyA+RNA using SMARTer® PCR cDNA Synthesis Kit (Takara Bio  
248 Inc., Shiga, Japan). The cDNA samples were size-fractionated with the BluePippin™  
249 system (Sage Science, MA, USA) and 700–1500 bp, 1500–3000 bp and 3000–6000 bp  
250 fractions were analysed with a PacBio®RSII sequencer (Pacific Biosciences, CA,  
251 U.S.A.). Iso-Seq-contigs were constructed using the RS\_IsoSeq protocol in SMRT  
252 Analysis (v2.3.0) with the parameter of estimated cDNA size. The *de novo* assembled  
253 RNA-seq-contigs and Iso-Seq-contigs were mapped to the genome by BLAT<sup>33</sup>, and  
254 each contig was annotated when at least 80% of its sequence was mapped. The mapped  
255 transcript data were used to make longer transcript models with PASA2 v. 2.0.2<sup>34</sup>.

256

257 **Annotation of repeat sequences.** Repeat sequences of *P. micropora* were identified

258 using the RepeatModeller package (v. open-1-0-8, <http://www.repeatmasker.org>) and  
259 masked by RepeatMasker v. 4.0<sup>27</sup>, using the identified-model repeat sequences and the  
260 repeat sequences of Repbase (ver. 20150807)<sup>35</sup> (<https://www.girinst.org/rebase/>). The  
261 model repeat sequences were annotated based on the sequence homology search against  
262 the NCBI nr database by BLASTX<sup>36</sup>. Representative Polintons and retrotransposons in  
263 Supplementary Table 3 were identified by manual inspection of the *P. micropora* draft  
264 genome aided by a sequence similarity search using BLAST software<sup>36</sup>.

265

266 **Gene annotation.** Protein genes of *P. micropora* were annotated by a combination of  
267 transcriptome-based gene modelling, *ab initio* gene prediction and protein  
268 homology-based gene prediction. In the transcriptome-based gene modelling, the  
269 transcripts were masked first by RepeatMasker because many spurious repetitive  
270 sequences, which were not removed by genome-repeat-masking, were detected. We  
271 discarded the transcript models when more than 80% of the region was masked by  
272 RepeatMasker. Exceptions were made when ORFs (> 50 aa) were predicted from the  
273 unmasked region. The ORFs and coding sequences of transcripts were predicted with

274 the Transdecoder Utility of Trinity<sup>37</sup>. *Ab initio* gene prediction was performed by  
275 Augustus<sup>38</sup>, whose training was performed using Iso-Seq data. Since *P. micropora*  
276 protein genes often contain simple repeat sequences in the exon regions, we avoided  
277 masking them for the *ab initio* gene prediction. The protein homology-based gene  
278 prediction was performed by Exonerate<sup>39</sup> after masking both the simple repeat and the  
279 interspersed repeat sequences, because the homology search in the presence of simple  
280 repeat sequences generated an extraordinary number of meaningless candidates (data  
281 not shown). In the Exonerate analysis, we used the protein sequences that passed the  
282 prescreening by BLASTX search (*P. micropora* genome vs. a local protein database  
283 composed of Uniprot and 4 rhizarian organisms, *B. natans*, *P. brassicae*, *P.*  
284 *chromatophore* and *R. filosa*). All gene models described above were combined, and the  
285 best one for each gene locus was chosen according to the bit score of the BLAST search,  
286 the presence/absence of transcript and ORF length. The quality of the genome assembly  
287 and the annotation was assessed by BUSCO v. 1<sup>40</sup>.

288

289 **Detection of DNA virus-like fragments.** Genomic segments with discernible

290 boundaries and distinct from the rest of the genome by the following four criteria were  
291 denoted as DNA virus-like fragments or putative DNA virus fragments: 1) repeat  
292 sequences detected by RepeatModeller but distinct from retrotransposons and the  
293 Maverick/Polinton-type transposons, 2) higher GC content, 3) large heterogeneous  
294 intron-less gene clusters and 4) ORFs similar to DNA virus proteins are encoded; DNA  
295 virus genes are found within the top 100 by BLASTP search against the NCBI nr  
296 database. The detailed procedure is as follows. Genomic scaffolds containing repeat  
297 sequences of the unknown class<sup>27</sup> were subjected to ORFfinder<sup>41</sup>, and ORFs detected  
298 were annotated by BLASTP<sup>36</sup> search against the NCBI nr database. The GC%  
299 distribution was analysed with CLC genomic workbench 7.0.3 (Qiagen). The virus copy  
300 number was analysed using the BLASTN<sup>36</sup> program searching the simple  
301 repeat-masked draft genome for virus coding sequences (Supplementary Table 3) or 100  
302 b fragments generated by slicing the virus-containing scaffolds (Fig. 3, Extended Data  
303 Fig. 6). BLASTN-redundant hits were manually removed.

304

305 **GO-term-, metabolism-pathway-, orthogroup- and protein-domain analysis.**

306 GO-terms were acquired by InterproScan 5<sup>42</sup>, and the enrichment analysis was  
307 performed by web-based Gostat<sup>43</sup> (<http://gostat.wehi.edu.au/>) using 27,653 GO-terms  
308 of 12,007 *P. micropora* genes and 88,634 GO-terms of 39,773 genes of 4 rhizarian  
309 organisms (*B. natans*, *P. brassicae*, *R. filosa* and *P. micropora*,). Metabolism-pathways  
310 were analysed using KAAS of KEGG<sup>44</sup> (<https://www.genome.jp/kegg/kaas/>).  
311 Orthogroup-analysis of Extended Data Fig. 3 was performed by Orthofinder<sup>45</sup> using a  
312 local protein database (Supplementary Table 10). Protein domain information in  
313 Extended Data Fig. 7 was acquired by NCBI conserved domain (CD) search  
314 (<https://www.ncbi.nlm.nih.gov/Structure/cdd/wrpsb.cgi>)<sup>46</sup>.  
315  
316 **nuclear-localized plastid DNA (nupDNA) and mitochondria DNA (numDNA)**  
317 **analysis.** Using the *P. micropora* plastid genome (DDBJ Accession No. LC490351) and  
318 mitochondria genome sequence (DDBJ Accession No. LC490352) for queries, nupDNA  
319 and numDNA were searched for by BLASTN against the *P. micropora* draft genome  
320 and the raw sequence reads of Illumina HiSeq2500. In the raw read-based nupDNA and  
321 numDNA analysis, chimeric segments of the organelle-like and non-organelle



322 sequences, which represent the junction region of nuclear localized organelle DNA,  
323 were surveyed. The detected reads were assembled by CodonCode Aligner (CodonCode  
324 Corporation, MA, U.S.A.). The chimera artefacts due to sequencing adaptors, or  
325 contaminated bacterial and mitochondria genomes, were identified by BLAST analysis  
326 using the NCBI database (nt, nr) and the mitochondria genome sequence (LC490352).

327

328 **Phylogenetic analysis and the divergent time analysis.** Multiple sequence alignment  
329 analyses were performed by MUSCLE<sup>47</sup> and MAFFT<sup>48</sup>. The phylogenetic trees were  
330 constructed using MEGA packages (version 6<sup>49</sup>, 7<sup>50</sup> and -CC<sup>51</sup>) and IQ-tree<sup>52</sup>. The  
331 divergent time analysis was performed using the RelTime method<sup>53</sup> implemented in  
332 MEGA 6. Parameters used for phylogenetic analyses are shown in Supplementary Table  
333 6 and 9, respectively.

334

335 **Analysis of EGT/HGT candidates.** *P. micropora* nuclear genes derived from  
336 cyanobacteria are referred to as EGT, and those derived from the rest of the bacteria are  
337 defined as HGT. To screen the EGT/HGT candidates, *P. micropora* MYN1 genes were

338 used as queries for the BLASTP search against the NCBI nr database with e-value  $\leq$   
339  $1e^{-10}$ , and top-hitting genes of the *Paulinella* plastid genes or prokaryotic protein  
340 sequences were selected. These genes were subjected to multiple alignment analyses by  
341 MUSCLE using the protein sequences of a local protein dataset in Supplementary Table  
342 10 and of the best BLASTP hit sequences. The obtained data sets were subjected to a  
343 neighbour joining (NJ) phylogenetic analysis (MEGA6, 7, CC) to choose *P. micropora*  
344 nuclear genes that form sister groups with prokaryotes or photosynthetic eukaryotes.  
345 After fine taxon re-samplings from the NCBI nr database, the NJ analysis selection was  
346 conducted again. The selected genes were finally subjected to maximum likelihood  
347 (ML) analysis using MEGA packages (MEGA6, 7, CC). *P. micropora* nuclear genes  
348 that satisfied at least one of the following three criteria were used as EGT and HGT  
349 candidates. 1) BLAST analysis of the gene gave no hint of eukaryote genes in the NCBI  
350 nr database. 2) EGT and HGT are supported by ML phylogenetic analysis with a high  
351 bootstrap value. We adopted a bootstrap value of 95 as threshold when phylogenetically  
352 available protein alignment sequence positions were long enough ( $\geq 100$  aa). We  
353 lowered the threshold to 70 when the available sites were less than 100 aa. 3) The gene

354 is included in the clade of photosynthetic organisms. To confirm the validity of the  
355 above mentioned EGT candidate selection, we also screened the EGT candidates by  
356 another independent procedure. The EGT candidates obtained by these two independent  
357 analyses were almost overlapping and, therefore, used for the analysis (Supplementary  
358 Table 6). The alternative analysis procedure is as follows. We performed a phylogenetic  
359 analysis using the software of multiple alignment (MAFFT) and ML phylogenetic  
360 analysis (IQ-tree), and alignment trimming tools (trimAI<sup>54</sup>, BMGE<sup>55</sup>). We selected  
361 genes hitting alpha-type cyanobacteria<sup>56,57</sup> within the top 100 by BLAST search against  
362 a custom database, which consists of the NCBI nr database supplemented with the  
363 protein sequences of 14 phylogenetically informative protists (Supplemental Table 10).

364

365 **Estimation of EGT/HGT timing.** To estimate the timing of EGT/HGT, we used *P.*  
366 *micropora* genes whose counter genes of *P. chromatophora* CCAC0185 were reported  
367 as EGT/HGT candidates<sup>58,59</sup>. In addition, we restricted the analysis to *Paulinella*  
368 ortholog's pairs that form a monophyletic sister group with a high bootstrap value ( $\geq$   
369 70). The nearest protein sequences of HGT/EGT candidates were surveyed from NCBI

370 nr database by BLASTP analysis. Within the top 2000 sequences of BLASTP hits, the  
371 phylogenetically nearest gene sequences were estimated using NJ and ML phylogenetic  
372 analysis. To estimate gene transfer timing, the branching time point when *P. micropora*  
373 MYN1 separated from the nearest non-rhizarian organisms in the ML phylogenetic tree  
374 was calculated using the RelTime method<sup>55</sup>. We used an estimated value of the  
375 divergence of *P. micropora* and *P. chromatophora* (45.7–64.7 MYA) based on the 18S  
376 rRNA phylogenetic tree corrected by fossil information<sup>11,60</sup>.

377

378 **Analysis of Mavericks/Polinton transposons.** *P. micropora*'s Mavericks/Polintons  
379 transposons were detected from the draft genome by tBLASTN using the sequence of  
380 the DNA polymerase (DNA-pol) domain. Thousands of DNA polymerase ORFs,  
381 predicted from the genome sequences by Transdecoder<sup>37</sup>, were subjected to NJ  
382 phylogenetic analyses. We grouped highly similar copies. Representative sequences that  
383 have long ORFs and less ambiguous amino acid residues were selected from each group  
384 and subjected to ML phylogenetic analysis.

385

386 **Divergent time analysis of the mobile elements.** In the divergent time analysis of  
387 Marvericks/Polintons DNA polymerases, representative DNA-pol sequences of *P.*  
388 *micropora* MYN1 Polintons having the traits of recent amplification (nucleotide  
389 sequence identity between the copies  $\geq 90\%$ ) were used. For the DNA-pol sequences of  
390 *P. chromatophora* CCAC0185 Polintons, the genome sequence-reads (SRR3217293.sra,  
391 SRR3217303.sra) were searched by BLASTX (e-value  $< 1e^{-20}$ ) using the sequence of *P.*  
392 *micropora* MYN1 Polintons, and then, the hit-reads were assembled into contigs with  
393 CLC Genomic Workbench 7.0 (Qiagen). For the analysis of virus-type GPCR genes, in  
394 addition to *P. micropora* MYN1 genes and *P. micropora* putative virus genes, the  
395 translated ORFs of *P. chromatophora* CCAC0185 transcripts were analysed. The GPCR  
396 gene family was detected by Orthofinder<sup>45</sup> and BLASTP<sup>36</sup> search. In this analysis, the  
397 genes encoding seven intact trans-membrane domain sequences, of which all seven  
398 trans-membrane helices can be identified by CD search<sup>46</sup>, were used. Furthermore,  
399 several genes predicted *ab initio* by Augustus without any supporting experimental data  
400 were removed from the analysis, because their gene models appeared to be artificial  
401 from applying eukaryotic splicing rules to virus-like fragments. The divergent time

402 points of the mobile elements and GPCR genes were calculated by setting the nearest  
403 branching point of *P. micropora* MYN1 and *P. chromatophora* CCAC0185 at 45.7–  
404 64.7 MYA.

405

#### 406 **Statistical analysis**

407 In GO-term enrichment analysis, Fisher's exact test (two tailed test) was performed and  
408 the p-values corrected with false discovery rate (Benjamini) were calculated. In the  
409 phylogenetic analysis, bootstrap test with  $\geq 100$  replicates was performed.

410

#### 411 **References**

412 1

413 Yoon, H.S., Hackett, J.D., Ciniglia, C., Pinto, G. & Bhattacharya, D. (2004) A  
414 molecular timeline for the origin of photosynthetic eukaryotes. *Mol. Biol. Evol.* **21**,  
415 809-18, <https://doi.org/10.1093/molbev/msh075> (2004).

416

417 2

418 Sánchez-Baracaldo, P., Raven, J. A., Pisani, D. & Knoll, A. H. Early photosynthetic  
419 eukaryotes inhabited low-salinity habitats. *Proc. Natl. Acad. Sci. USA* **114**,  
420 E7737-E7745. <https://doi.org/10.1073/pnas.1620089114> (2017).

421

422 3

423 McFadden, G. I. Origin and evolution of plastids and photosynthesis in eukaryotes.  
424 *CSH Perspect Biol.* **6**, a016105, <https://doi.org/10.1101/cshperspect.a016105> (2014).

425

426 4

427 Burki, F. & Keeling, P. J. Rhizaria. *Curr. Biol.* **24**, R103-R107,  
428 <https://doi.org/10.1016/j.cub.2013.12.025> (2014).

429

430 5

431 Nomura, M., Nakayama, T. & Ishida, K. Detailed process of shell construction in the  
432 photosynthetic testate amoeba *Paulinella chromatophora* (euglyphid, Rhizaria). *J.*  
433 *Eukaryot. Microbiol.* **61**. 317-321. <https://doi.org/10.1111/jeu.12102> (2014).

434

435 6

436 Matsuo, M. *et al.* Characterization of spliced leader trans-splicing in a photosynthetic

437 rhizarian amoeba, *Paulinella micropora*, and its possible role in functional gene transfer.

438 *PLoS One* **13**, e0200961, <https://doi.org/10.1371/journal.pone.0200961> (2018).

439

440 7

441 Nowack, E. C., Melkonian, M. & Glöckner, G. Chromatophore genome sequence of

442 *Paulinella* sheds light on acquisition of photosynthesis by eukaryotes. *Curr. Biol.* **18**,

443 410-418, <https://doi.org/10.1016/j.cub.2008.02.051> (2008).

444

445 8

446 Yoon, H. S. *et al.* A single origin of the photosynthetic organelle in different *Paulinella*

447 lineages. *BMC Evol. Biol.* **9**, 98, <https://doi.org/10.1186/1471-2148-9-98> (2009).

448

449 9



450 Reyes-Prieto, A. *et al.* Differential gene retention in plastids of common recent origin.

451 *Mol. Biol. Evol.* **27**, 1530-1537, <https://doi.org/10.1093/molbev/msq032> (2010).

452

453 10

454 Nakayama, T. & Ishida, K. Another acquisition of a primary photosynthetic organelle is

455 underway in *Paulinella chromatophora*. *Curr. Biol.* **19**, R284-R285,

456 <https://doi.org/10.1016/j.cub.2009.02.043> (2009).

457

458 11

459 Delaye, L., Valadez-Cano, C. & Pérez-Zamorano, B. (2016) How Really Ancient Is

460 *Paulinella Chromatophora*? *PLOS Curr. Tree. Life.*

461 <https://doi.org/10.1371/currents.tol.e68a099364bb1a1e129a17b4e06b0c6b> (2016).

462

463 12

464 Martin, W. *et al.* Evolutionary analysis of Arabidopsis, cyanobacterial, and chloroplast

465 genomes reveals plastid phylogeny and thousands of cyanobacterial genes in the

466 nucleus. *Proc. Natl. Acad. Sci. USA.* **99**, 12246-12251,

467 <https://doi.org/10.1073/pnas.182432999> (2002).

468

469 13

470 Koonin, E. V. & Yutin, N. Evolution of the Large Nucleocytoplasmic DNA Viruses of

471 Eukaryotes and Convergent Origins of Viral Gigantism. *Adv. Virus Res.* **103**, 167-202,

472 <https://doi.org/10.1016/bs.aivir.2018.09.002> (2019).

473

474 14

475 Komenda, J. & Sobotka, R. Cyanobacterial high-light-inducible proteins--Protectors of

476 chlorophyll-protein synthesis and assembly. *Biochim. Biophys. Acta.* **1857**, 288-295,

477 <https://doi.org/10.1016/j.bbabi.2015.08.011> (2016).

478

479 15

480 Matsuo, M., Ito, Y., Yamauchi, R. & Obokata, J. The rice nuclear genome continuously

481 integrates, shuffles, and eliminates the chloroplast genome to cause chloroplast-nuclear

482 DNA flux. *Plant Cell* **17**, 665-675, <https://doi.org/10.1105/tpc.104.027706> (2005).

483

484 16

485 Smith, D. R., Crosby, K. & Lee, R. W. Correlation between nuclear plastid DNA  
486 abundance and plastid number supports the limited transfer window hypothesis.

487 *Genome Biol. Evol.* **3**, 365-71, <https://doi.org/10.1093/gbe/evr001> (2011).

488

489 17

490 Bhattacharya, D. *et al.* Single cell genome analysis supports a link between phagotrophy  
491 and primary plastid endosymbiosis. *Sci Rep.* **2**, 356, <https://doi.org/10.1038/srep00356>  
492 (2012).

493

494 18

495 Feschotte, C. & Pritham, E. J. Non-mammalian c-integrases are encoded by giant  
496 transposable elements. *Trends Genet.* **21**, 551-552,  
497 <https://doi.org/10.1016/j.tig.2005.07.007> (2005).

498

499 19

500 Kapitonov, V. V. & Jurka, J. Self-synthesizing DNA transposons in eukaryotes. *Proc.*

501 *Natl. Acad. Sci. USA* **103**, 4540-4545, <https://doi.org/10.1073/pnas.0600833103> (2006).

502

503 20

504 Koonin, E. V. & Yutin, N. Multiple evolutionary origins of giant viruses. *F1000Res.* **7**,

505 F1000 Faculty Rev-1840, <https://doi.org/10.12688/f1000research.16248.1> (2018).

506

507 21

508 Fischer, M. G. & Suttle, C. A. A virophage at the origin of large DNA transposons.

509 *Science* **332**, 231-234, <https://doi.org/10.1126/science.1199412> (2011).

510

511 22

512 La Scola, B. *et al.* The virophage as a unique parasite of the giant mimivirus. *Nature*

513 **455**, 100-104. <https://doi.org/10.1038/nature07218> (2008).

514

515 23

516 Fischer, M. G. & Hackl, T. Host genome integration and giant virus-induced

517 reactivation of the virophage mavirus. *Nature* **540**, 288-291.

518 <https://doi.org/10.1038/nature20593> (2016).

519

520 24

521 Blanc, G., Gallot-Lavallée, L. & Maumus, F. Provirophages in the *Bigelowiella* genome

522 bear testimony to past encounters with giant viruses. *Proc. Natl. Acad. Sci. USA* **112**,

523 E5318-5326, <https://doi.org/10.1073/pnas.1506469112> (2015).

524

525 25

526 Boyer, M. *et al.* Giant Marseillevirus highlights the role of amoebae as a melting pot in

527 emergence of chimeric microorganisms. *Proc. Natl. Acad. Sci. USA* **106**, 21848-21853,

528 <https://doi.org/10.1073/pnas.0911354106> (2009).

529

530 26

531 Piskurek, O. & Okada, N. Poxviruses as possible vectors for horizontal transfer of  
532 retroposons from reptiles to mammals. *Proc. Natl. Acad. Sci. USA* **104**, 12046-12051  
533 <https://doi.org/10.1073/pnas.0700531104> (2007).

534

535 27

536 Smit, AFA, Hubley, R. & Green, P. *RepeatMasker Open-4.0*. 2013-2015,  
537 <http://www.repeatmasker.org>.

538

539 **Method-only references**

540 28

541 Luo, R. *et al.* SOAPdenovo2: an empirically improved memory-efficient short-read de  
542 novo assembler. *GigaScience* **1**, 18, <https://doi.org/10.1186/2047-217X-1-18> (2012).

543

544 29

545 Marçais, G. & Kingsford, C. A fast, lock-free approach for efficient parallel counting of

546 occurrences of k-mers. *Bioinformatics* **27**, 764–770,  
547 <https://doi.org/10.1093/bioinformatics/btr011> (2011).

548

549 30

550 Grabherr, M. G. et al. Full-length transcriptome assembly from RNA-Seq data without a  
551 reference genome. *Nat. Biotechnol.* **29**, 644–652, <https://doi.org/10.1038/nbt.1883>  
552 (2011).

553

554 31

555 Trapnell C., Pachter L. & Salzberg, S. L. TopHat: discovering splice junctions with  
556 RNA-Seq. *Bioinformatics* **25**, 1105–1111, <https://doi.org/10.1093/bioinformatics/btp120>  
557 (2009).

558

559 32

560 Trapnell, C. *et al.* Transcript assembly and quantification by RNA-Seq reveals  
561 unannotated transcripts and isoform switching during cell differentiation. *Nat.*

562 *Biotechnol.* **28**, 511–515, <https://doi.org/10.1038/nbt.1621> (2010).

563

564 33

565 Kent W. J. BLAT--the BLAST-like alignment tool. *Genome Res.* **12**, 656-664,

566 <https://doi.org/10.1101/gr.229202> (2002).

567

568 34

569 Haas, B.J. *et al.* Improving the Arabidopsis genome annotation using maximal

570 transcript alignment assemblies. *Nucleic Acids Res.* **31**, 5654-5666,

571 <https://doi.org/10.1093/nar/gkg770> (2003).

572

573 35

574 Bao, W., Kojima, K. K., & Kohany, O. Repbase Update, a database of repetitive

575 elements in eukaryotic genomes. *Mob. DNA* **6**, 11,

576 <https://doi.org/10.1186/s13100-015-0041-9> (2015).

577



578 36

579 Camacho C. *et al.* BLAST+: architecture and applications. *BMC Bioinformatics* **10**, 421,  
580 <https://doi.org/10.1186/1471-2105-10-421> (2009).

581

582 37

583 Haas, B.J. *et al.* De novo transcript sequence reconstruction from RNA-seq using the  
584 Trinity platform for reference generation and analysis. *Nat. Protoc.* **8**, 1494-1512,  
585 <https://doi.org/10.1038/nprot.2013.084> (2013).

586

587 38

588 Stanke, M., Diekhans, M., Baertsch, R. & Haussler, D. Using native and syntenically  
589 mapped cDNA alignments to improve de novo gene finding. *Bioinformatics* **24**, 637–  
590 644, <https://doi.org/10.1093/bioinformatics/btn013> (2008).

591

592 39

593 Slater, G. S. & Birney, E. Automated generation of heuristics for biological sequence

594 comparison. *BMC Bioinformatics* **6**, 31, <https://doi.org/10.1186/1471-2105-6-31> (2005).

595

596 40

597 Simão, F. A., Waterhouse, R. M., Ioannidis, P., Kriventseva, E. V. & Zdobnov E. M.

598 BUSCO: assessing genome assembly and annotation completeness with single-copy

599 orthologs. *Bioinformatics* **31**, 3210-3212, <https://doi.org/10.1093/bioinformatics/btv351>

600 (2015).

601

602 41

603 David, L. *et al.* Database resources of the National Center for Biotechnology. *Nucleic*

604 *Acids Res.* **31**, 28–33, <https://doi.org/10.1093/nar/gkg033> (2003).

605

606 42

607 Jones, P. *et al.* InterProScan 5: genome-scale protein function classification.

608 *Bioinformatics* **30**, 1236–1240, <https://doi.org/10.1093/bioinformatics/btu031> (2014).

609

610 43

611 Beissbarth, T. & Speed, T. P. Gostat: Find statistically overrepresented Gene  
612 Ontologies within a group of genes. *Bioinformatics* **20**, 1464-1465,  
613 <https://doi.org/10.1093/bioinformatics/bth088> (2004).

614

615 44

616 Moriya, Y., Itoh, M., Okuda, S., Yoshizawa, A., & Kanehisa, M. KAAS: an automatic  
617 genome annotation and pathway reconstruction server. *Nucleic Acids Res.* **35**,  
618 W182-W185, <https://doi.org/10.1093/nar/gkm321> (2007).

619

620 45

621 Emms, D. M. & Kelly S. OrthoFinder: solving fundamental biases in whole genome  
622 comparisons dramatically improves orthogroup inference accuracy. *Genome Biol.* **16**,  
623 157, <https://doi.org/10.1186/s13059-015-0721-2> (2015).

624

625 46

626 Marchler-Bauer, A. et al. CDD/SPARCLE: functional classification of proteins via  
627 subfamily domain architectures. *Nucleic Acids Res.* **45**, D200-D203,  
628 <https://doi.org/10.1093/nar/gkw1129> (2017).

629

630 47

631 Edgar R. C. MUSCLE: multiple sequence alignment with high accuracy and high  
632 throughput. *Nucleic Acids Res.* **32**, 1792-1797, <https://doi.org/10.1093/nar/gkh340>  
633 (2004).

634

635 48

636 Katoh, K., Misawa, K., Kuma, K. & Miyata T. MAFFT: a novel method for rapid  
637 multiple sequence alignment based on fast Fourier transform. *Nucleic Acids Res.* **30**,  
638 3059-3066, <https://doi.org/10.1093/nar/gkf436> (2002).

639

640 49

641 Tamura, K., Stecher, G., Peterson, D., Filipowski, A. & Kumar, S. MEGA6: Molecular

642 Evolutionary Genetics Analysis Version 6.0. *Mol. Biol. Evol.* **30**, 2725-2729,

643 <https://doi.org/10.1093/molbev/mst197> (2013).

644

645 50

646 Kumar, S., Stecher, G., & Tamura, K. (2016) MEGA7: Molecular Evolutionary

647 Genetics Analysis Version 7.0 for bigger datasets. *Mol. Biol. Evol.* **33**, 1870-1874,

648 <https://doi.org/10.1093/molbev/msw054> (2016).

649

650 51

651 Kumar, S., Stecher, G., Peterson, D. & Tamura, K. MEGA-CC: Computing Core of

652 Molecular Evolutionary Genetics Analysis Program for Automated and Iterative Data

653 Analysis. *Bioinformatics* **28**, 2685-2686, <https://doi.org/10.1093/bioinformatics/bts507>

654 (2012).

655

656 52

657 Nguyen, L.-T., Schmidt, H.A., von Haeseler, A. & Minh, B.Q. IQ-TREE: A fast and

658 effective stochastic algorithm for estimating maximum likelihood phylogenies. *Mol.*  
659 *Biol. Evol.* **32**, 268-274, <https://doi.org/10.1093/molbev/msu300> (2015).

660

661 53

662 Tamura, K, Tao, Q. & Kumar S. Theoretical Foundation of the RelTime Method for  
663 Estimating Divergence Times from Variable Evolutionary Rates. *Mol. Biol. Evol.* **35**,  
664 1770–1782, <https://doi.org/10.1093/molbev/msy044> (2018).

665

666 54

667 Capella-Gutiérrez S., Silla-Martínez, J. M. & Gabaldón, T. trimAl: a tool for automated  
668 alignment trimming in large-scale phylogenetic analyses. *Bioinformatics* **25**, 1972-1973,  
669 <https://doi.org/10.1093/bioinformatics/btp348> (2009).

670

671 55

672 Criscuolo, A. & Gribaldo, S. BMGE (Block Mapping and Gathering with Entropy): a  
673 new software for selection of phylogenetic informative regions from multiple sequence

674 alignments. *BMC Evol. Biol.* **10**, 210, <https://doi.org/10.1186/1471-2148-10-210> (2010).

675

676 56

677 Badger M. R., Hanson, D. & Price G. D. Evolution and diversity of CO<sub>2</sub> concentrating

678 mechanisms in cyanobacteria. *Funct. Plant Biol.* **29**, 161–173,

679 <https://doi.org/10.1071/PP01213> (2002).

680

681 57

682 Marin, B., Nowack, E. C., Glöckner, G. & Melkonian, M. The ancestor of the Paulinella

683 chromatophore obtained a carboxysomal operon by horizontal gene transfer from a

684 Nitrococcus-like gamma-proteobacterium. *BMC Evol. Biol.* **7**, 85,

685 <https://doi.org/10.1186/1471-2148-7-85> (2007).

686

687 58

688 Nowack, E. C. *et al.* Gene transfers from diverse bacteria compensate for reductive

689 genome evolution in the chromatophore of Paulinella chromatophora. *Proc. Natl. Acad.*

690 *Sci. USA* **113**, 12214-12219, <https://doi.org/10.1073/pnas.1608016113> (2016).

691

692 59

693 Nowack, E. C. et al. Endosymbiotic gene transfer and transcriptional regulation of

694 transferred genes in *Paulinella chromatophora*. *Mol. Biol. Evol.* **28**, 407-422,

695 <https://doi.org/10.1093/molbev/msq209> (2011).

696

697 60

698 Lhee, D. *et al.* Diversity of the Photosynthetic *Paulinella* Species, with the Description

699 of *Paulinella micropora* sp. nov. and the Chromatophore Genome Sequence for strain

700 KR01. *Protist* **168**, 155–170, <https://doi.org/10.1016/j.protis.2017.01.003> (2017).

701

702

### 703 **Acknowledgements**

704 We thank Dr. Terabayashi T. for his kind instructions in SEM analysis.

705 Computations were partially performed on the NIG supercomputer at ROIS National



706 Institute of Genetics. This work was supported by JSPS KAKENHI grants: 221S0002,  
707 15K14554, 1 and 6K14788, and by a Grant-in-Aid for Scientific Research on  
708 Innovative Areas 3308 of the Ministry of Education, Culture, Sports, Science and  
709 Technology of Japan.

710

#### 711 **Author contributions**

712 M. M. prepared the *P. micropora* MYN1 genome samples, identified the  
713 putative virus sequence in the *P. micropora* MYN1 genome and wrote the draft  
714 manuscript. M. M. and A. K. performed the RNA sample preparation. Y. M., H. N., A.  
715 T. and A. F. performed the genome sequencing, the genome assembly and the Iso-Seq  
716 analysis. Y. S. performed the RNA-seq sequencing analysis. M. N. and K. I. cultured *P.*  
717 *micropora* MYN1. M. M., A. K., M. T., H. N., H. T., S. S., M. N. and K. I. annotated  
718 the *P. micropora* MYN1 genome. M. M., T. N. and R. K. performed the phylogenetic  
719 analysis. T. N., R. K. and Y. I. analysed the organelle (chromatophore, mitochondria)  
720 genome. J. O. organized and managed the *P. micropora* MYN1 genome project and  
721 finalized the manuscript. We thank the members of Comparative Genomics

722 Laboratory in National Institute of Genetics for technical and computational  
723 assistance.

724

725 **Competing interests**

726 The authors declare no competing interests.

727

728 **Materials & Correspondence**

729 Junichi Obokata

730 Email: [obokata@kpu.ac.jp](mailto:obokata@kpu.ac.jp)

731 Tel/Fax: +81-75-703-5164

732 Graduate School of Life and Environmental Science,

733 Kyoto Prefectural University, Kyoto, 606-8522, Japan

734

735

736

737

738 **Figure Legends**

739 **Fig. 1. An overview of the *P. micropora* MYN1 draft genome. a,** A SEM image of *P.*  
740 *micropora* MYN1. **b,** The statistics of the draft genome. **c,** The genome composition of  
741 *P. micropora* MYN1 analysed by RepeatMasker<sup>27</sup>. **d,** Simple repeats are extraordinarily  
742 rich in *P. micropora* MYN1 compared with other organisms.

743

744 **Fig. 2. *P. micropora* nuclear genes acquired by EGT/HGT. a, b,** A functional  
745 classification of the *P. micropora* nuclear genes derived from cyanobacteria (EGT  
746 candidates) (**a**), and those from other bacteria (HGT candidates) (**b**). **c, d,** The amino  
747 acid sequence identity of EGT candidates against *P. micropora* MYN1 plastid genes (**c**)  
748 and that of HGT candidates against bacterial genes of the NCBI nr database (**d**). **e, f,** An  
749 estimation of the gene transfer age for EGT candidates (**e**) and HGT candidates (**f**). The  
750 endosymbiosis initiation period is green-highlighted. The ages of gene transfer in (**e**)  
751 and (**f**) were calculated based on the divergent time points (45.7–64.7 MYA) of two  
752 *Paulinella* species; thus, a gene transfer age younger than 60 MYA (striped phase)  
753 could not be estimated.

754

755 **Fig. 3. Putative DNA virus and mobile elements in *P. micropora* MYN1. a, A**  
756 schematic view of DNA virus-like fragments and mobile elements in the *P. micropora*  
757 draft genome (Scaffold 1104). The genomic regions were coloured according to the  
758 sequence characteristics; putative dsDNA virus (pink), Polinton (light blue),  
759 retrotransposon (brass yellow) and simple repeat-rich region (grey). The copy number  
760 of the interspersed repeat elements was analysed by BLASTN against the  
761 simple-repeat-masked *P. micropora* draft genome. **b**, ML phylogenetic tree of DNA  
762 polymerases of viruses, eukaryotes and prokaryotes. **c**, Divergent time analysis of the  
763 virus-type GPCR in *Paulinella*'s lineage. **d**, **e**, Divergent time analysis of DNA  
764 polymerase genes of metazoa-type (**d**) and rhizarian-type (**e**) Polintons. Asterisks: the  
765 branch point of *P. micropora* and *P. chromatophora* set at 45.7–64.7 MYA. Green  
766 bands: initiation periods of endosymbiosis with cyanobacteria (93.6–141.4 MYA). *P.*  
767 *micropora*; *Paulinella micropora* MYN1, *P. chromatophora*; *Paulinella*  
768 *chromatophora* CCAC0185, *P. brassicae*; *Plasmodiophora brassicae*, *R. filosa*;  
769 *Reticulomyxa filosa*, *S. purpurus*; *Strongylocentrotus purpuratus*.

770

771 **Fig. 4. Initial process of the endosymbiotic evolution of photosynthetic *Paulinella***  
772 **species modeled from the *P. micropora* genomic data. 1)** Predacious ancestors  
773 digested prey bacteria via phagocytosis with continuing low levels of HGT. **2)** The  
774 infection of large DNA virus triggered the massive HGT/EGT to promote the rapid  
775 endosymbiotic evolution. **3)** Acquiring photosynthetic competency shrunk the  
776 phagocytic activity to shut down the source of HGT/EGT. **4)** The photo-autotrophic  
777 *Paulinella* sp. contains one photosynthetic organelle per cell, hence, release of the  
778 organelle DNA hardly occurred without losing photosynthetic activity. In this final  
779 stage, virus-mediated gene transfer continued at trace level.

780

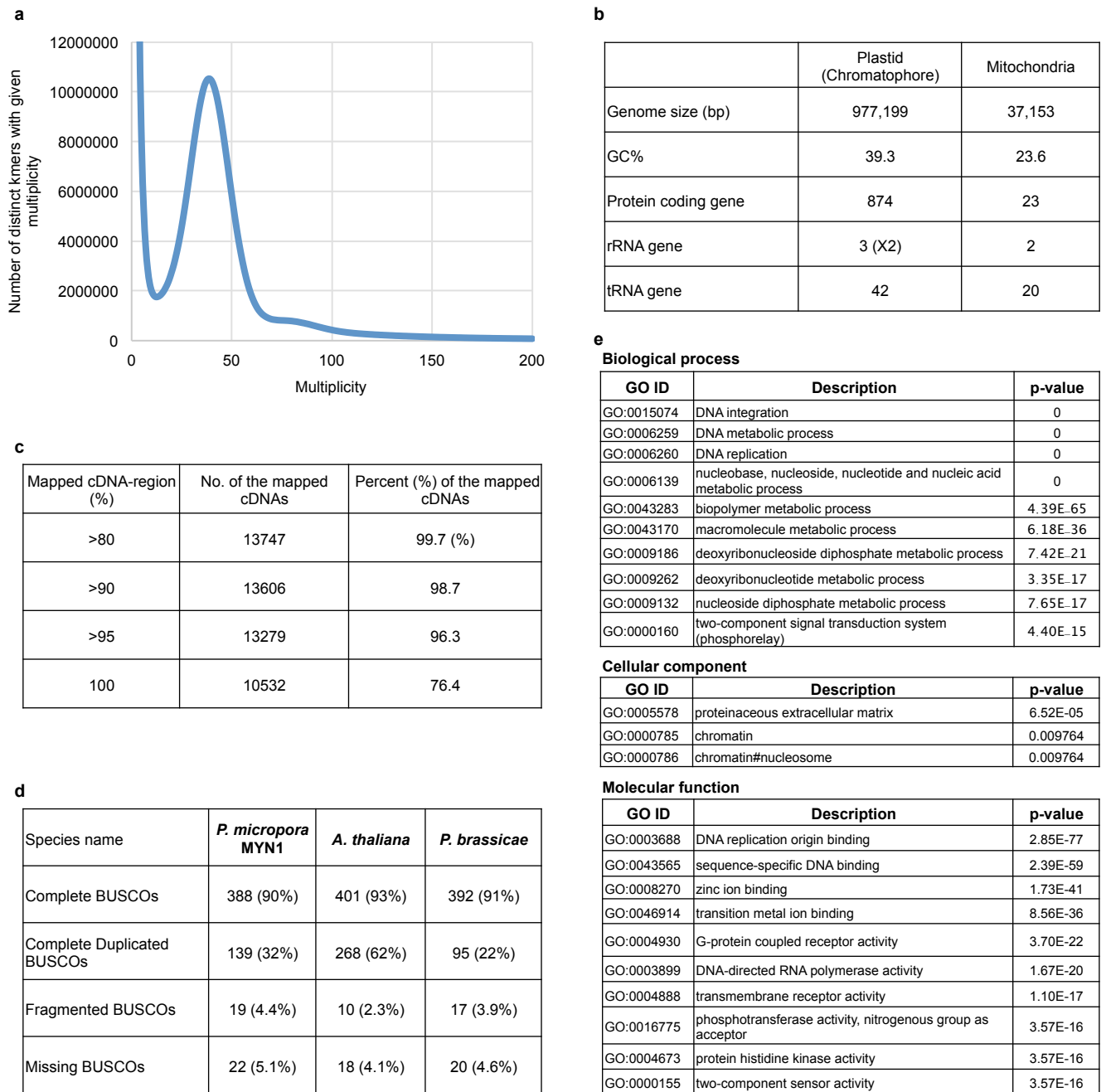
781

782

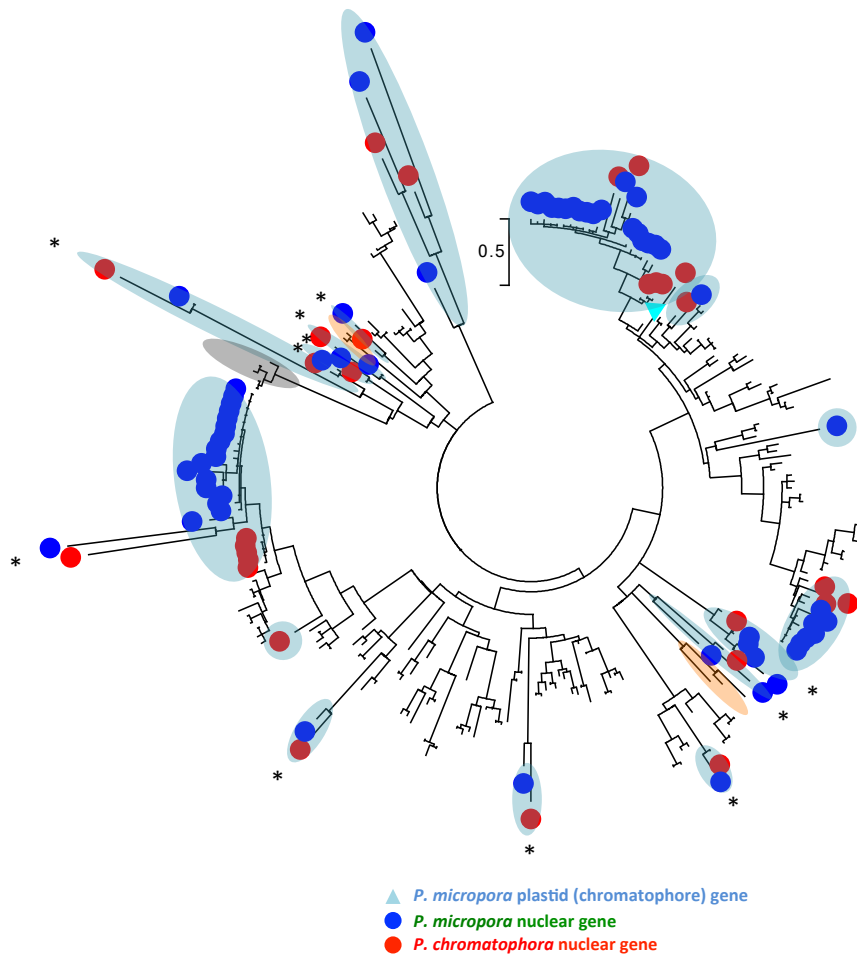
783

784

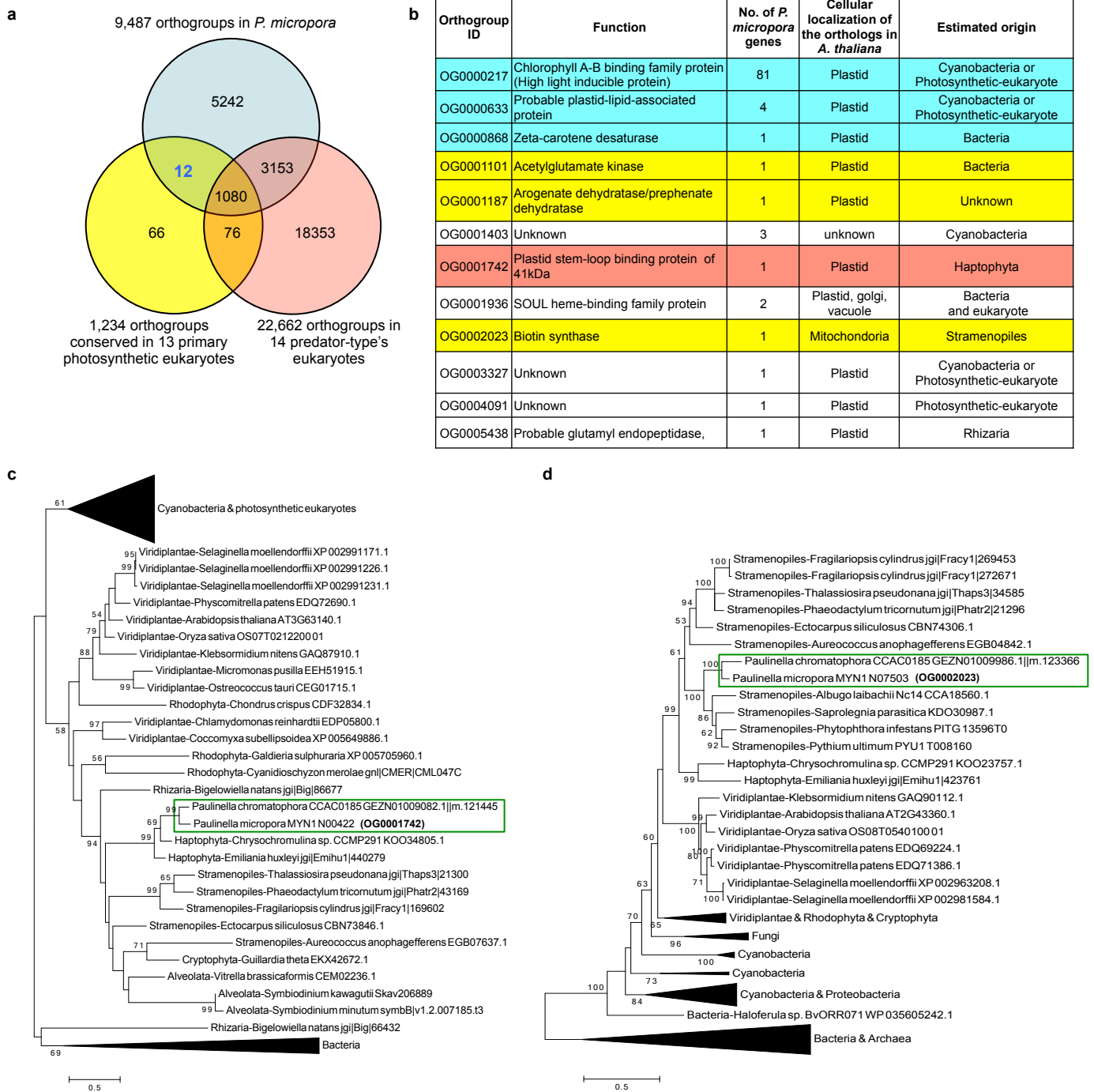
785



**Extended Data Fig. 1. Information of the *P. micropora* MYN1 genome.** **a**, Estimation of the *P. micropora* MYN1 genome by K-mer frequency analysis. Single peak at 39 of the multiplicity are detected with 31-mer, utilizing 52,592,411,100 b from Illumina 500b pair-end reads. From the peak value and the used reads length, 1.35 Gb genome size was estimated. **b**, Summary of the *P. micropora* MYN1 organelle genome. **c**, Validation of the genome assembly by mapping of the sequences of the isoform sequencing (Iso-Seq) transcripts. 13787 non-redundant Iso-Seq sequences of the intron-containing genes, either hitting protein sequences of the Swiss-Prot database by BLASTX search (e-value  $\leq 1e^{-60}$ ) or containing long ORFs ( $\geq 300$  amino acids), were mapped on the draft genome. **d**, Assessment of the genome assembly using 429 BUSCO v. 1 (Benchmarking Universal Single-Copy Orthologs) genes. In comparison with other eukaryote genome assemblies, the BUSCO values of a photosynthetic organism (*Arabidopsis thaliana*) and that of the well-assembled genome of a rhizarian organism (*Plasmodiophora brassicae*) are shown. **e**, The top 10 GO-terms that are significantly overrepresented in the *P. micropora* MYN1 genome compared with other rhizarian organisms (*Bigelowiella natans*, *Plasmodiophora brassicae*, *Reticulomyxa filosa*). Fisher's exact test p-values corrected with false discovery rate (Benjamini) are represented.



**Extended Data Fig. 2.** A ML phylogenetic tree of Hlips of *P. micropora* MYN1 and *P. chromatophora*. Hlips of cyanobacteria, photosynthetic eukaryotes and cyanophages are used as a reference for operational taxonomy units. Sixty-four *P. micropora* Hlip genes were subjected to phylogenetic analysis and grouped according to the clade. The redundant paralogs of identical sequences were removed. Asterisks: *Paulinella* ortholog-pair supported by a bootstrap value >70. Blue and red circle: nuclear encoded Hlip of *P. micropora* and *P. chromatophora*. Light-blue triangle: *P. micropora* plastid (chromatophore) Hlip. Phylogenetic branch of the *Paulinella* gene (light blue), virus (grey) and eukaryote Hlip-like gene (orange) are highlighted.



**Extended Data Fig. 3. Comparison of the orthogroups of *P. micropora*, primary photosynthetic eukaryotes and predator-type eukaryotes.** **a**, Venn diagram of *P. micropora* orthogroups with the predator-type eukaryote orthogroups and the conserved orthogroups in primary photosynthetic eukaryotes. Orthogroups were detected by Orthofinder from the gene sets of *P. micropora* MYN1, 14 predator eukaryotes (*Acanthamoeba castellanii*, *Dictyostelium discoideum*, *Entamoeba histolytica* HM-1, *Bodo saltans*, *Naegleria gruberi*, *Caenorhabditis elegans*, *Drosophila melanogaster*, *Monosiga brevicollis* MX1, *Oxytricha trifallax*, *Paramecium tetraurelia*, *Stylonychia lemnae*, *Tetrahymena thermophila*, *Reticulomyxa filosa*, *Thecamonas trahens* ATCC50062) and 13 photosynthetic eukaryotes (*Arabidopsis thaliana*, *Chlamydomonas reinhardtii*, *Coccomyxa subellipsoidea* C-169, *Klebsormidium nitens*, *Micromonas pusilla* CCMP1545, *Oryza sativa*, *Ostreococcus tauri*, *Physcomitrella patens*, *Selaginella moellendorffii*, *Chondrus crispus*, *Cyanidioschyzon merolae*, *Galdieria sulphuraria*, *Cyanophora paradoxa*). **b**, Annotations of 12 orthogroups conserved in primary photosynthetic eukaryotes, but not in predator eukaryotes. The functional annotation and the cellular localization were based on UniprotKB information of *Arabidopsis thaliana* orthologs, and manual annotations are represented in parenthesis. The estimated origins were based on the ML phylogenetic analysis. Genes involved in light acclimation (cyan), nutrient auxotrophy (yellow) and organelle gene expression (magenta) are highlighted. **c** and **d**, ML phylogenetic trees of orthogroup genes acquired by HGT from other eukaryotes; Haptophyta (**c**, OG0001742) and Stramenopiles (**d**, OG0002023). The phylogenetic analysis of **c** and **d** were performed using a LG+G (**c**) and a LG+G+I model (**d**), respectively. Photosynthetic *Paulinella* species are boxed.



**a**

**Analysis flow of nupDNA and numDNA with Illumina paired-end reads**

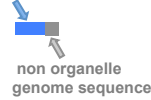
① **Detection of the reads similar to plastid- and mitochondria-genome**

BLASTN hit (e-value  $\leq 1e-10$ )

BLAST Database sequence  
*P. micropora* plastid genome  
*P. micropora* mitochondria genome  
 Two contaminated bacteria genome

| No. of Candidates  |                   |
|--------------------|-------------------|
| nupDNA             | numDNA            |
| 14,272,422 (reads) | 3,019,020 (reads) |

② **Chimeric reads having at least 5b non-organelle genome sequence (organelle genome like sequence)**



|                |                |
|----------------|----------------|
| 57,845 (reads) | 32,824 (reads) |
|----------------|----------------|

③ **The reads whose pair are less similar to the organelle genome**

BLASTN hit length < 100b or the sequence identity < 95%



|               |               |
|---------------|---------------|
| 6,821 (reads) | 9,236 (reads) |
|---------------|---------------|

④ **The junction contigs, assembled with at least 5 reads**



|              |              |
|--------------|--------------|
| 35 (contigs) | 58 (contigs) |
|--------------|--------------|

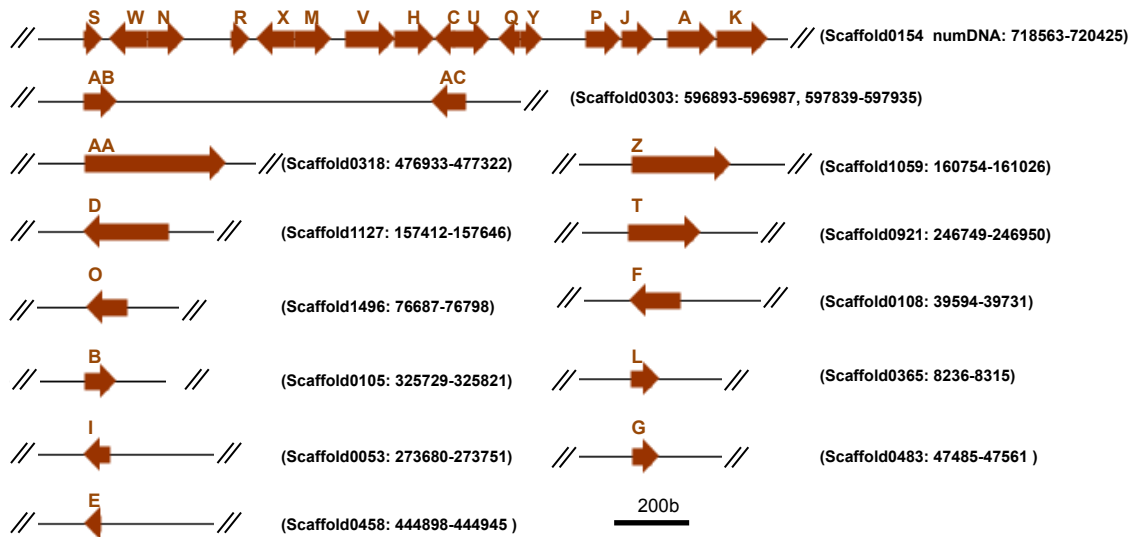
⑤ **nupDNA- and numDNA-contigs after removal of the contamination**

**Contaminants**

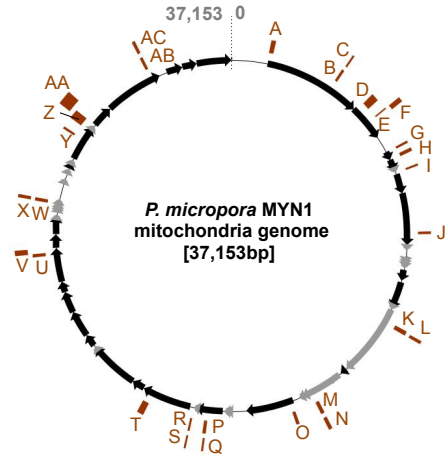
- Bacteria genomes
- Mitochondria genome variants
- Artificial sequences fused to HiSeq-adaptor sequence

|             |              |
|-------------|--------------|
| 0 (contigs) | 42 (contigs) |
|-------------|--------------|

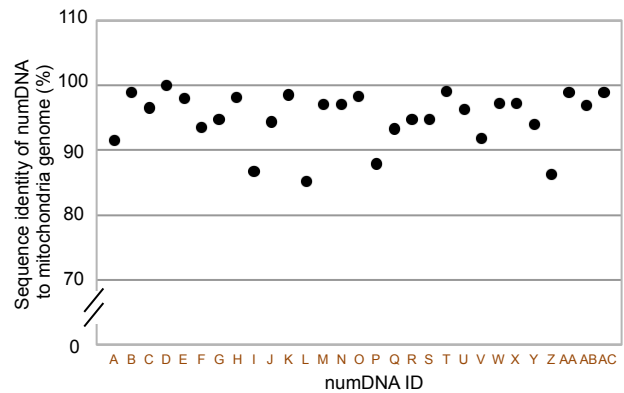
**b**



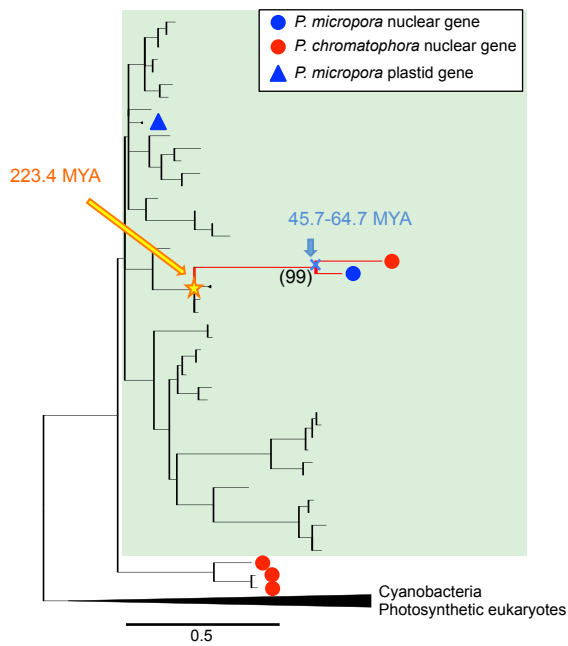
**c**



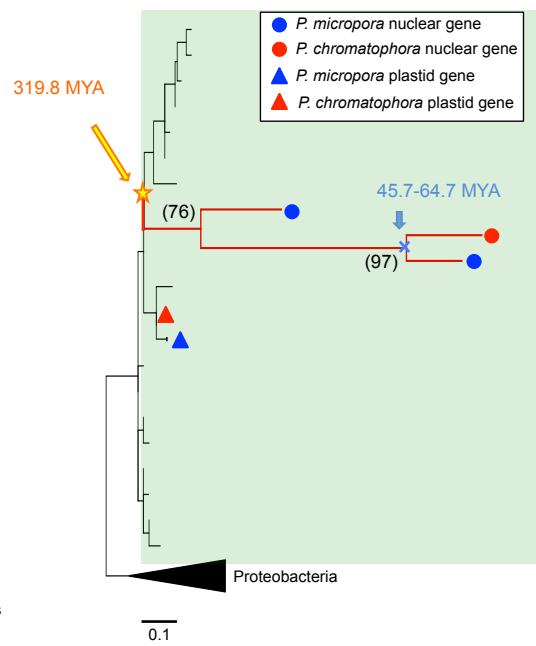
**d**



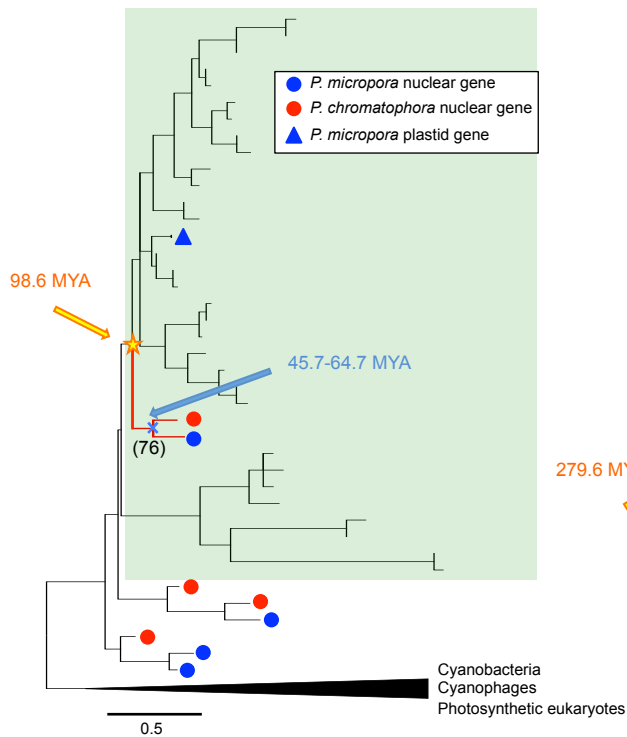
PsaK; N18495 [LG+G+I]



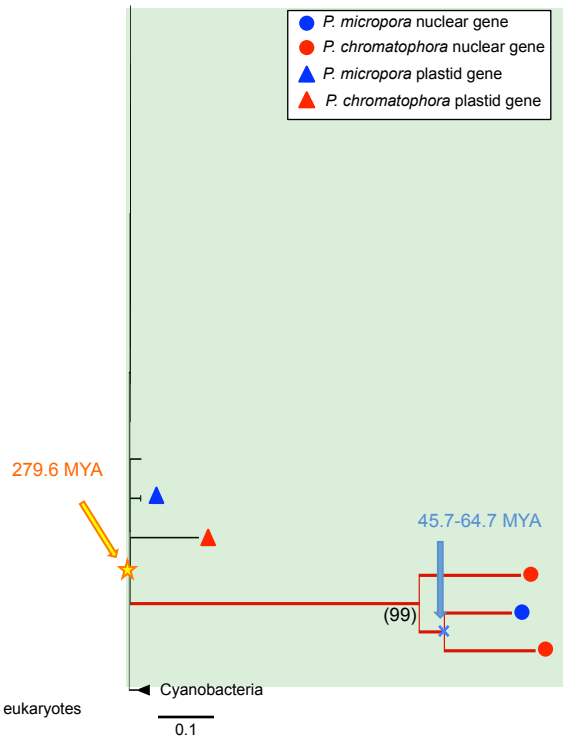
CcmL; N15137, N17777 [rtREV+G]



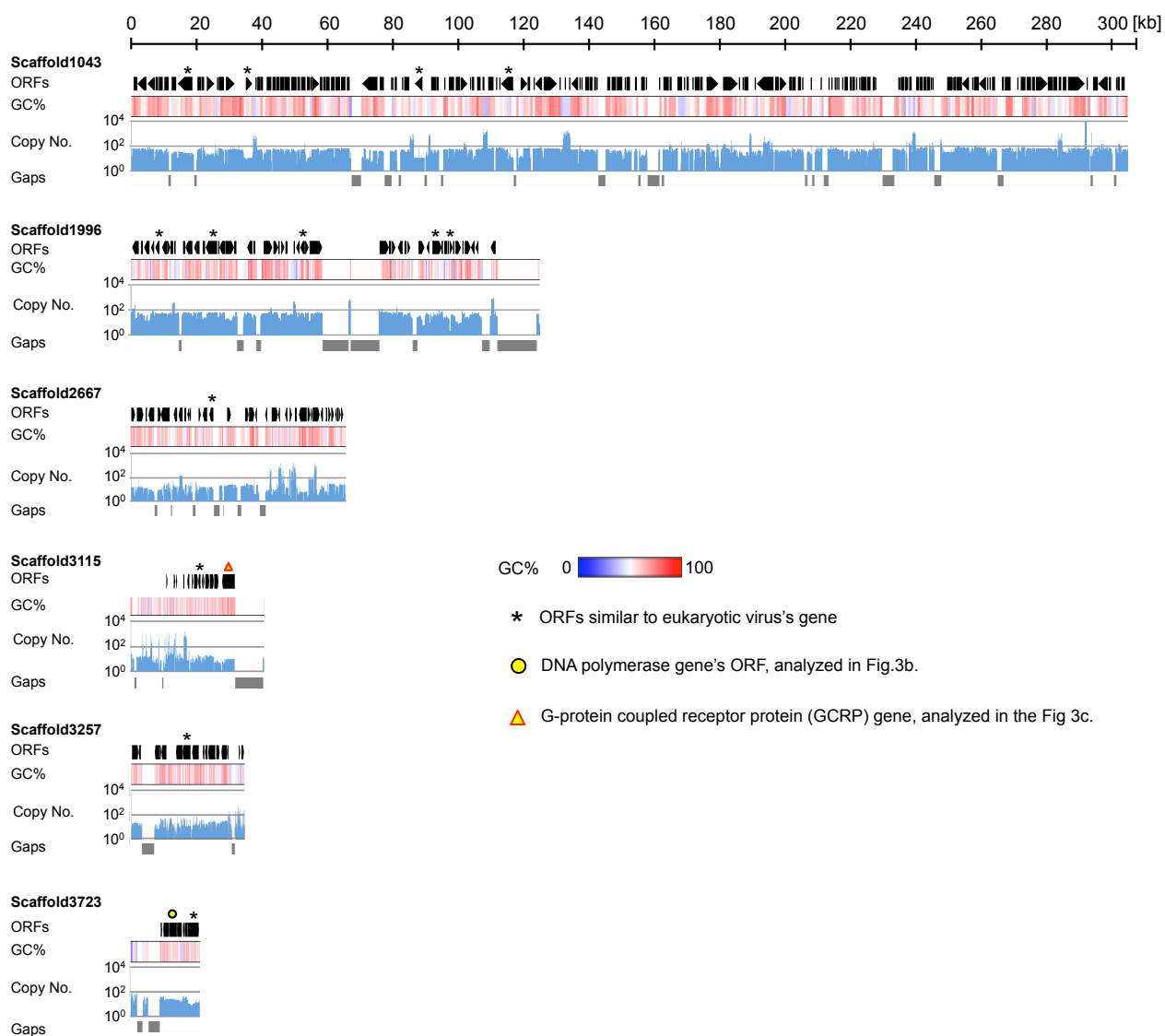
Hlip; N30377 [LG+G]



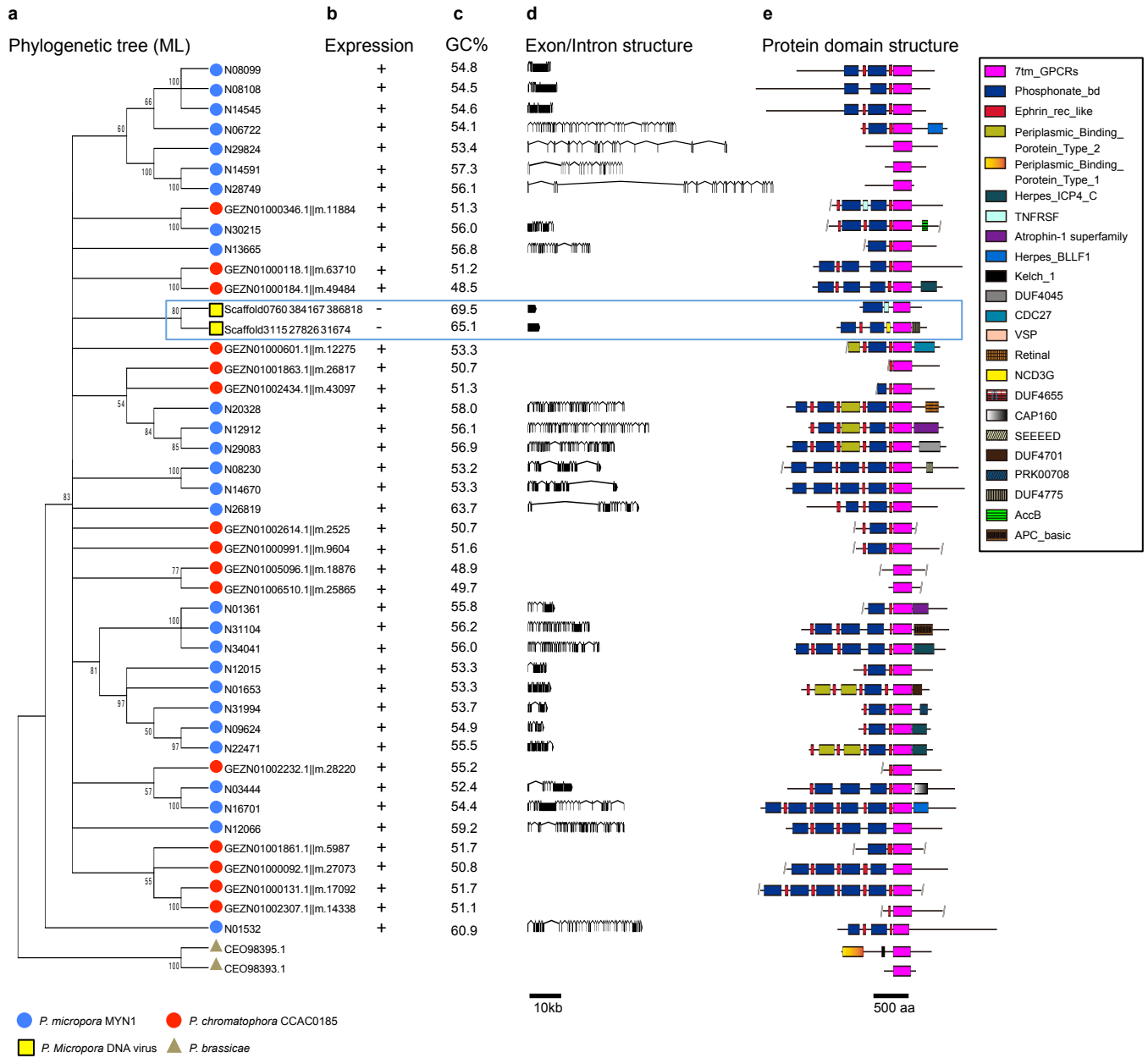
Hypothetical protein; N11415 [LG+I]



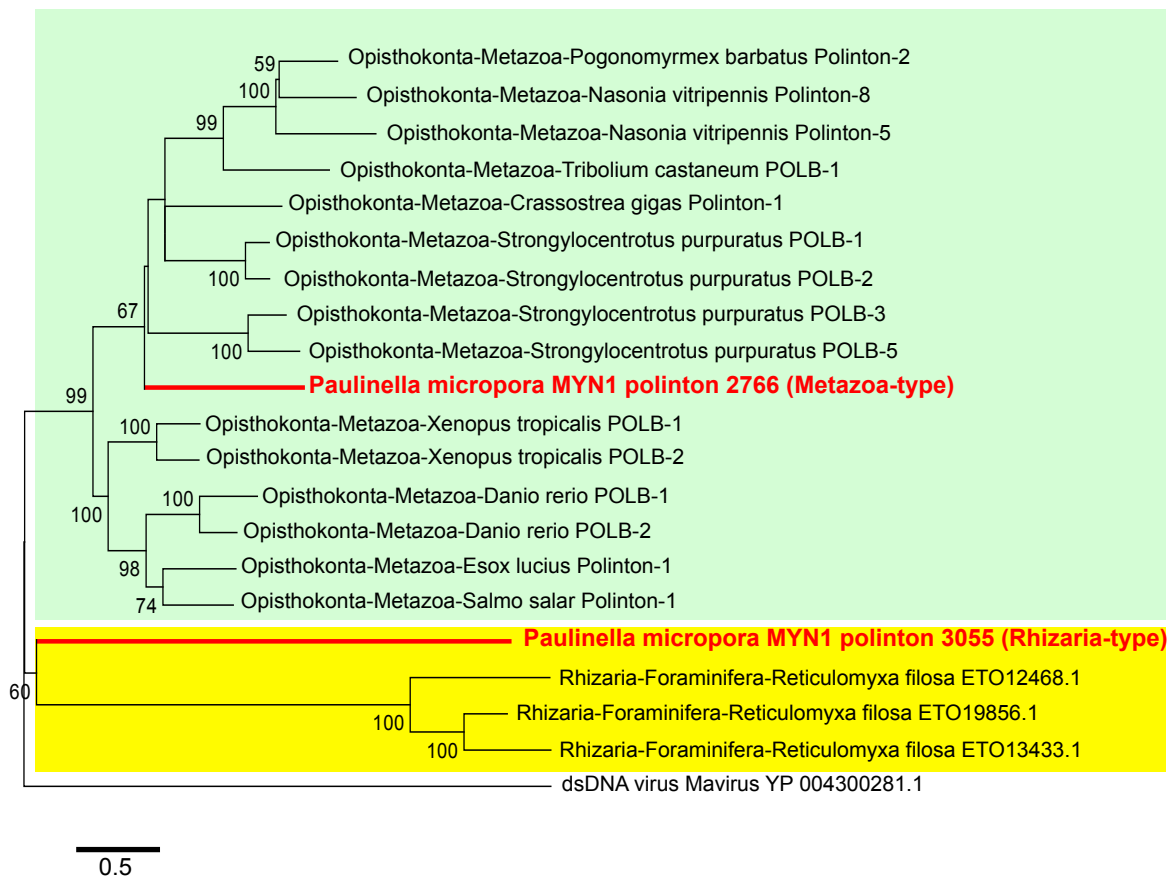
**Extended Data Fig. 5. ML phylogenetic trees of four EGT candidates whose counterpart orthologs are found in the plastid (chromatophore) genome of *P. micropora*.** The clades of the *Paulinella* plastid and cyanobacteria are highlighted in green. Blue circle: *P. micropora* nuclear gene, red circle: *P. chromatophora* nuclear gene, blue triangle: *P. micropora* plastid gene, red triangle: *P. chromatophora* plastid gene, unmarked: cyanobacterium gene. The branch of *P. micropora* and *P. chromatophora* nuclear genes supported by high bootstraps (numbers in the parenthesis) is represented as a red line. The divergence time of *Paulinella* nuclear genes from the plastid- or other cyanobacterial-genes (yellow stars) were estimated by RelTime methods of MEGA6 using the divergent time of *P. micropora* and *P. chromatophora* (45.7–64.7 MYA) (blue cross). PsaK: Photosystem I subunit K, CcmL: CO<sub>2</sub> concentrating mechanism protein, Hlip: High light inducible protein. Brackets mean the substitution model used in the phylogenetic analysis. Trees with species names are available at the repository (<https://figshare.com/s/a665678c48d0af073894>).



**Extended Data Fig. 6. Putative DNA virus fragments detected in the *P. micropora* draft genome.** ORF structures, GC%, copy number and sequence gaps are represented as described in the legend to Fig. 3.



**Extended Data Fig. 7. Characteristics of virus-type GPCRs of *P. micropora* and *P. chromatophora*.** **a**, A ML phylogenetic tree of seven transmembrane domains of GPCRs. GPCRs in *P. micropora*, *P. chromatophora*, *P. brassicae* (CEO98393.1, CEO98395.1), and those detected in DNA viral fragments were analysed using a LG+G+F model. Branches with bootstrap values <50 are condensed. **b**, Existence of the transcript. **c**, GC% of the coding sequence of GPCR genes. **d**, Exon/intron structures of the genes. **e**, Protein domain structures. Protein domains were detected by CD search<sup>48</sup>. GPCRs in putative DNA viruses are boxed with a blue line.



**Extended Data Fig. 8. ML phylogenetic tree of DNA polymerases of Polintons. a,** DNA polymerase sequences of *P. micropora* Polintons (No. 2766 and No. 3055), *R. filosa* Polintons (Genbank, ETO12468.1, ETO19856.1, ETO13433.1), metazoan Polintons in Rebase<sup>37</sup> and Mavirus (Genbank, YP 004300281.1) were analysed with a LG+G+I model. The metazoan and rhizarian groups are highlighted in green and yellow, respectively.

786 **Extended Data legends**

787 **Extended Data Fig. 1. Information of the *P. micropora* MYN1 genome. a,**

788 Estimation of the *P. micropora* MYN1 genome size by K-mer frequency analysis.

789 Single peak at 39 of the multiplicity are detected with 31-mer, utilizing 52,592,411,100

790 b from Illumina 500b pair-end reads. From the peak value and the used reads length,

791 1.35 Gb genome size was estimated. **b,** Summary of the *P. micropora* MYN1 organelle

792 genome. **c,** Validation of the genome assembly by mapping of the sequences of the

793 isoform sequencing (Iso-Seq) transcripts. 13787 non-redundant Iso-Seq sequences of

794 the intron-containing genes, either hitting protein sequences of the Swiss-Prot database

795 by BLASTX search (e-value  $\leq 1e^{-60}$ ) or containing long ORFs ( $\geq 300$  amino acids),

796 were mapped on the draft genome. **d,** Assessment of the genome assembly using 429

797 BUSCO v. 1 (Benchmarking Universal Single-Copy Orthologs) genes. In comparison

798 with other eukaryote genome assemblies, the BUSCO values of a photosynthetic

799 organism (*Arabidopsis thaliana*) and that of the well-assembled genome of a rhizarian

800 organism (*Plasmodiophora brassicae*) are shown. **e,** The top 10 GO-terms that are

801 significantly overrepresented in the *P. micropora* MYN1 genome compared with other

802 rhizarian organisms (*Bigelowiella natans*, *Plasmodiophora brassicae*, *Reticulomyxa*  
803 *filosa*). Fisher's exact test p-values corrected with false discovery rate (Benjamini) are  
804 represented.

805

806 **Extended Data Fig. 2. A ML phylogenetic tree of Hlips of *P. micropora* MYN1 and**  
807 ***P. chromatophora*.** Hlips of cyanobacteria, photosynthetic eukaryotes and cyanophages  
808 are used as a reference for operational taxonomy units. Sixty-four *P. micropora* Hlip  
809 genes were subjected to phylogenetic analysis and grouped according to the clade. The  
810 redundant paralogs of identical sequences were removed. Asterisks: *Paulinella*  
811 ortholog-pair supported by a bootstrap value >70. Blue and red circle: nuclear encoded  
812 Hlip of *P. micropora* and *P. chromatophora*. Light-blue triangle: *P. micropora* plastid  
813 (chromatophore) Hlip. Phylogenetic branch of the *Paulinella* gene (light blue), virus  
814 (grey) and eukaryote Hlip-like gene (orange) are highlighted.

815

816 **Extended Data Fig. 3. Comparison of the orthogroups of *P. micropora*, primary**  
817 **photosynthetic eukaryotes and predator-type eukaryotes. a,** Venn diagram of *P.*

818 *micriopora* orthogroups with the predator-type eukaryote orthogroups and the  
819 conserved orthogroups in primary photosynthetic eukaryotes. Orthogroups were  
820 detected by Orthofinder from the gene sets of *P. micropora* MYN1, 14 predator  
821 eukaryotes (*Acanthamoeba castellanii*, *Dictyostelium discoideum*, *Entamoeba*  
822 *histolytica* HM-1, *Bodo saltans*, *Naegleria gruberi*, *Caenorhabditis elegans*,  
823 *Drosophila melanogaster*, *Monosiga brevicollis* MX1, *Oxytricha trifallax*, *Paramecium*  
824 *tetraurelia*, *Stylonychia lemnae*, *Tetrahymena thermophila*, *Reticulomyxa filosa*,  
825 *Thecamonas trahens* ATCC50062) and 13 photosynthetic eukaryotes (*Arabidopsis*  
826 *thaliana*, *Chlamydomonas reinhardtii*, *Coccomyxa subellipsoidea* C-169,  
827 *Klebsormidium nitens*, *Micromonas pusilla* CCMP1545, *Oryza sativa*, *Ostreococcus*  
828 *tauri*, *Physcomitrella patens*, *Selaginella moellendorffii*, *Chondrus crispus*,  
829 *Cyanidioschyzon merolae*, *Galdieria sulphuraria*, *Cyanophora paradoxa*). **b**,  
830 Annotations of 12 orthogroups conserved in primary photosynthetic eukaryotes, but not  
831 in predator eukaryotes. The functional annotation and the cellular localization were  
832 based on UniprotKB information of *Arabidopsis thaliana* orthologs, and manual  
833 annotations are represented in parenthesis. The estimated origins were based on the ML



834 phylogenetic analysis. Genes involved in light acclimation (cyan), nutrient auxotrophy  
835 (yellow) and organelle gene expression (magenta) are highlighted. **c** and **d**, ML  
836 phylogenetic trees of orthogroup genes acquired by HGT from other eukaryotes;  
837 Haptophyta (**c**, OG0001742) and Stramenopiles (**d**, OG0002023). The phylogenetic  
838 analysis of **c** and **d** were performed using a LG+G (**c**) and a LG+G+I model (**d**),  
839 respectively. Photosynthetic *Paulinella* species are boxed.

840

841 **Extended Data Fig. 4. Analysis of nuclear-localized plastid DNA (nupDNA) and**  
842 **mitochondria DNA (numDNA) in *P. micropora*.** **a**, Analysis of the junction sequences  
843 of nupDNA and numDNA using Illumina raw-reads sequences. 902,121,079  
844 quality-trimmed HiSeq paired-end sequence reads (insert size: 300 b, 500 b) were  
845 analysed. **b**, numDNA sequence structures in the *P. micropora* draft genome. **c**,  
846 Distribution of numDNA sequences in mitochondrial genome positions. **d**, Nucleotide  
847 percent identity of numDNA compared with the mitochondria genome sequence.  
848 NumDNA directions are represented by right and left arrows which denote clockwise-  
849 and anti-clockwise directions of the mitochondria genome sequence (**c**), respectively.

850

851 **Extended Data Fig. 5. ML phylogenetic trees of four EGT candidates whose**  
852 **counterpart orthologs are found in the plastid (chromatophore) genome of *P.***  
853 ***micropora*.** The clades of the *Paulinella* plastid and cyanobacteria are highlighted in  
854 green. Blue circle: *P. micropora* nuclear gene, red circle: *P. chromatophora* nuclear  
855 gene, blue triangle: *P. micropora* plastid gene, red triangle: *P. chromatophora* plastid  
856 gene, unmarked: cyanobacterium gene. The branch of *P. micropora* and *P.*  
857 *chromatophora* nuclear genes supported by high bootstraps (numbers in the parenthesis)  
858 is represented as a red line. The divergence time of *Paulinella* nuclear genes from the  
859 plastid- or other cyanobacterial-genes (yellow stars) were estimated by RelTime  
860 methods of MEGA6 using the divergent time of *P. micropora* and *P. chromatophora*  
861 (45.7–64.7 MYA) (blue cross). Psak: Photosystem I subunit K, CcmL: CO<sub>2</sub>  
862 concentrating mechanism protein, Hlip: High light inducible protein. Brackets mean the  
863 substitution model used in the phylogenetic analysis. Trees with species names are  
864 available at the repository (<https://figshare.com/s/a665678c48d0af073894>).

865

866 **Extended Data Fig. 6. Putative DNA virus fragments detected in the *P. micropora***  
867 **draft genome.** ORF structures, GC%, copy number and sequence gaps are represented  
868 as described in the legend to Fig. 3.

869

870 **Extended Data Fig. 7. Characteristics of virus-type GPCRs of *P. micropora* and *P.***  
871 ***chromatophora*.** **a,** A ML phylogenetic tree of seven transmembrane domains of  
872 GPCRs. GPCRs in *P. micropora*, *P. chromatophora*, *P. brassicae* (CEO98393.1,  
873 CEO98395.1), and those detected in DNA viral fragments were analysed using a  
874 LG+G+F model. Branches with bootstrap values <50 are condensed. **b,** Existence of the  
875 transcript. **c,** GC% of the coding sequence of GPCR genes. **d,** Exon/intron structures of  
876 the genes. **e,** Protein domain structures. Protein domains were detected by CD search<sup>48</sup>.  
877 GPCRs in putative DNA viruses are boxed with a blue line.

878

879 **Extended Data Fig. 8. ML phylogenetic tree of DNA polymerases of Polintons. a,**  
880 DNA polymerase sequences of *P. micropora* Polintons (No. 2766 and No. 3055), *R.*  
881 *filosa*' Polintons (Genbank, ETO12468.1, ETO19856.1, ETO13433.1), metazoan

882 Polintons in Repbase<sup>37</sup> and Mavirus (Genbank, YP 004300281.1) were analysed with a  
883 LG+G+I model. The metazoan and rhizarian groups are highlighted in green and yellow,  
884 respectively.

885

886

### 887 **Supplementary information**

888 **Supplementary Table 1. Summary of the raw sequence data of the *P. micropora***  
889 **genome.**

890

891 **Supplementary Table 2. Annotation and categorization of the *P. micropora***

892 **RepeatModeller sequences.** \*The categorization is based on the sequence similarities

893 with the manually curated repeat sequences in Supplementary Table 3 by BLASTX

894 search (e-value < 1e<sup>-5</sup>).

895

896 **Supplementary Table 3. Annotation of the repeat elements manually identified**

897 **from the *P. micropora* draft genome.** \*The copy number of the repeat elements was

898 estimated by BLASTN search against the *P. micropora* genome. Redundant BLASTN  
899 hits at the same genome locus were manually removed.

900

901 **Supplementary Table 4. *P. micropora* MYN1 gene list.**

902

903 **Supplementary Table 5. GO-terms over- and under-represented in the *P.***

904 ***micropora* MYN1 genome compared with the genome of other rhizarian organisms**

905 **(*B. natans*, *P. brassicae* and *R. filosa*).** Significantly enriched GO-terms with Fisher's

906 exact test p-value less than 0.01 are represented.

907

908 **Supplementary Table 6. EGT and HGT candidates in *P. micropora* MYN1.** Genes

909 satisfying at least one of the following criteria were considered as EGT and HGT

910 candidates. 1) No hits to eukaryote genes of the NCBI nr database by BLAST analysis\*

911 2) EGT and HGT are supported by ML phylogenetic analysis with a high bootstrap

912 value ( $\geq 95$ ) except when the phylogenetically available protein alignment sequences

913 were short ( $< 100$  amino acids)\*\* 3) *P. micropora* genes were embedded in the clade of

914 photosynthetic organisms in the phylogenetic tree. \* BLASTP top 1000 hits (NCBI nr,  
915 e-value <  $1e^{-10}$ ) were classified. A: Archaea, B: Bacteria, E: Eukaryotes, V: Viruses, O:  
916 Others, U: Unknown. \*\* We lowered the threshold of the bootstrap value to 70 when  
917 the alignment sequence positions available for the phylogenetic analysis were less than  
918 100 amino acids.

919

920 **Supplementary Table 7. Detection of *P. micropora* Polintons by tBLASTn search**

921 **using DNA polymerase domain sequences.** A tBLASTn search was performed against

922 the *P. micropora* draft genome (e-value <  $1e^{-10}$ ). The draft genome sequences and the

923 query sequences are available at the repository

924 (<https://figshare.com/s/a665678c48d0af073894>).

925

926 **Supplementary Table 8. Accession numbers of *P. micropora* MYN1 genome**

927 **sequences.**

928

929 **Supplementary Table 9. Parameters of the ML phylogenetic analysis by MEGA6.**

930

931 **Supplementary Table 10. Sequence data used in this study.**

932

933

934

935

936

937

938

939

940

941

942

943

944

945